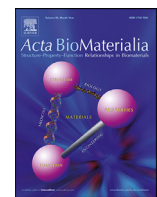




Contents lists available at ScienceDirect

Acta Biomaterialia

journal homepage: [www.elsevier.com/locate/actbio](http://www.elsevier.com/locate/actbio)

## Review article

## Control strategies of ice nucleation, growth, and recrystallization for cryopreservation

Min Lin <sup>a,b</sup>, Haishan Cao <sup>a,b,\*</sup>, Junming Li <sup>a,b</sup><sup>a</sup> Key Laboratory for Thermal Science and Power Engineering of Ministry of Education, Tsinghua University, Beijing 100084, China<sup>b</sup> Beijing Key Laboratory for CO<sub>2</sub> Utilization and Reduction Technology, Tsinghua University, Beijing 100084, China

## ARTICLE INFO

## Article history:

Received 23 August 2022

Revised 20 October 2022

Accepted 26 October 2022

Available online xxx

## Keywords:

Cryopreservation

Control strategies

Nucleation

Growth

Recrystallization

## ABSTRACT

The cryopreservation of biomaterials is fundamental to modern biotechnology and biomedicine, but the biggest challenge is the formation of ice, resulting in fatal cryoinjury to biomaterials. To date, abundant ice control strategies have been utilized to inhibit ice formation and thus improve cryopreservation efficiency. This review focuses on the mechanisms of existing control strategies regulating ice formation and the corresponding applications to biomaterial cryopreservation, which are of guiding significance for the development of ice control strategies. Herein, basics related to biomaterial cryopreservation are introduced first. Then, the theoretical bases of ice nucleation, growth, and recrystallization are presented, from which the key factors affecting each process are analyzed, respectively. Ice nucleation is mainly affected by melting temperature, interfacial tension, shape factor, and kinetic prefactor, and ice growth is mainly affected by solution viscosity and cooling/warming rate, while ice recrystallization is inhibited by adsorption or diffusion mechanisms. Furthermore, the corresponding research methods and specific control strategies for each process are summarized. The review ends with an outlook of the current challenges and future perspectives in cryopreservation.

## Statement of significance

Ice formation is the major limitation of cryopreservation, which causes fatal cryoinjury to cryopreserved biomaterials. This review focuses on the three processes related to ice formation, called nucleation, growth, and recrystallization. The theoretical models, key influencing factors, research methods and corresponding ice control strategies of each process are summarized and discussed, respectively. The systematic introduction on mechanisms and control strategies of ice formation is instructive for the cryopreservation development.

© 2022 Acta Materialia Inc. Published by Elsevier Ltd. All rights reserved.

## 1. Introduction

The global organ shortage for transplantation has been considered a major public health challenge and only 10% of patients receive organ transplants, as the World Health Organization estimates [1,2]. One major reason resulting in this crisis lies in organ ischemia injury *in vitro*, leading to short survival times and massive waste [3,4]. Currently, to prolong the storage time of biomaterials and alleviate organ shortages, the preservation of biomaterials is imperative [5]. Besides, preservation technologies have also been widely utilized in biomedicine and biotechnology, such as cell ther-

apy, tissue engineering, and biobank [6]. Hence, an in-depth study of cryopreservation is vital for basic research and clinical applications of biomedical science.

The fundamental principles of most preservation methods are based on temperature reduction [2], which realizes long-term preservation by slowing temperature-dependent biological metabolism described by Arrhenius kinetics [7]. According to the difference in storage temperature, there are several categories of preservation technologies (Fig. 1A): hypothermic preservation, supercooling preservation, and cryopreservation (including freezing preservation and vitrification), respectively. Hypothermic preservation is the most prevalent method of clinical organ preservation [8–10]. The organs to be preserved are immersed in preservation solution and maintained at 0~4 °C, decreasing cellular metabolism and providing cytoprotection [9]. However, the preservation time

\* Corresponding author.

E-mail address: [HaishanCao@tsinghua.edu.cn](mailto:HaishanCao@tsinghua.edu.cn) (H. Cao).

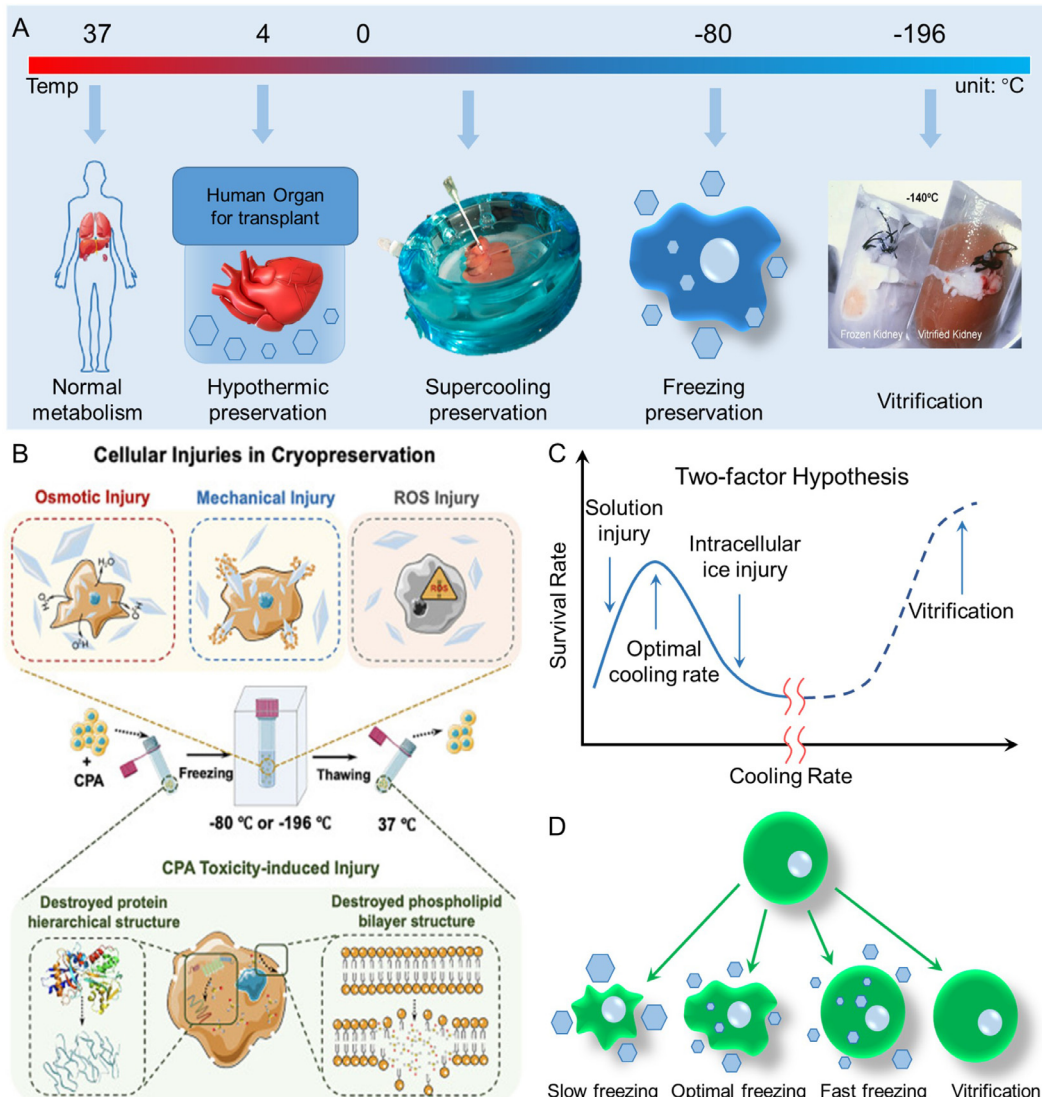


**Fig. 1.** Biomaterials preservation methods and cellular injuries in cryopreservation. (A) Four commonly used biomaterials preservation methods and their preservation temperature [7]. (B) Cellular injuries in cryopreservation, include ice-induced osmotic injury, mechanical injury, reactive oxygen species (ROS) injury, and CPA toxicity-induced injury [10]. (C) The two-factor hypothesis of cellular injury. (D) Cell volume response and injuries corresponding to cooling rates [20].

is still limited to a few hours, typically 4 h for hearts and lungs; 8~12 h for livers, and up to 36 h for kidneys [5,11]. Supercooling preservation is the method by which biomaterials enter a supercooled state to avoid ice injury because the phase transition does not immediately occur when the temperature reaches subzero for hydrated biomaterials [12–14]. However, the supercooled state is metastable and it is easy to induce crystallization with minimal thermal and physical disturbance, which will cause serious mechanical damage [15]. Besides, it is more difficult to maintain the supercooled state for large irregular biomaterials.

By contrast, cryopreservation, usually at -80~−196 °C, can achieve long-term storage theoretically [11,16–18], following the Arrhenius equation. However, there exist several cellular injuries suffered by biomaterials during cryopreservation [10,19] (Fig. 1B) and the greatest challenge is the fact that biomaterials consist primarily of water in a physiological saline solution, which undergoes the inevitable transformation from liquid water to ice crystals at sub-zero temperatures, resulting in fatal and irreversible damage to biomaterials [20]. To attenuate adverse effects and obtain a high survival rate of biomaterials during cryopreservation, cryoprotective agents (CPAs) are often used empirically when cooling

biomaterials to sub-zero temperatures [21]. Cryopreservation can be divided into freezing preservation and vitrification according to the cooling rate [17]. Freezing preservation is commonly used for the preservation of mammalian cells, with cooling rates of about  $1\text{ }^{\circ}\text{C min}^{-1}$  [22]. Despite the existence of low CPA solutions, ice crystals (including extracellular and intracellular ice) still inevitably form and affect cell survival rates. For the injury mechanism during freezing preservation, the most widely accepted is the “two-factor hypothesis” theory proposed by Mazur et al. [15,23]. As illustrated in Fig. 1C and 1D, the extracellular solution nucleates first due to the driving force of supercooling, affecting intracellular water migration and the formation of intracellular ice. When the cooling rate is extremely slow, intracellular water flows out from the cell membrane since the osmotic pressure of intracellular water is lower than that of the extracellular solution, leading to the dehydration of cells, called the solute effect. With the increase in cooling rate, intracellular water cannot penetrate into the external solution at once, resulting in the formation of fatal intracellular ice when subcooling is sufficient, called intracellular ice injury. However, with respect to intracellular ice formation, the underlying mechanisms are still controversial. The main theories

that elucidate the intracellular ice formation mechanisms include the pore theory (the intracellular ice is seeded by the extracellular ice through aqueous pores in the cell membranes [24]), surface-catalyzed nucleation and volume-catalyzed nucleation (the intracellular ice is a result of undercooling catalyzed by either the cell membranes via the effects of the extracellular ice, called surface-catalyzed nucleation, or the intracellular particles, called volume-catalyzed nucleation or homogeneous nucleation [25]), and cell membrane damage theory (the intracellular ice is seeded by the extracellular ice due to damage to the cell membranes caused by electrical transients [26] or osmotic pressures [27]). No matter whether extracellular ice or intracellular ice causes damage to cryopreserved cells, ice control strategies, referring to the specific method that can regulate ice formation, should be utilized for optimizing ice formation and minimizing ice injury. Generally, the pattern of traditional freezing preservation is to obtain the highest survival rate by analyzing the comprehensive influence of different factors empirically, such as cooling rate, CPA type, CPA concentration, and preservation temperature.

Vitrification is supposed to be an alternative method of cryopreservation, in which cell fluid does not transform into crystal ice but amorphous ice [11,28–31]. In this method, biomaterials can theoretically be stored indefinitely under the glass transition temperature of the solution, and no need to worry about ice injury. Unfortunately, there are still several obstacles to the realization of vitrification. Firstly, an extremely fast cooling/warming rate is required to avoid ice recrystallization and devitrification, and the critical warming rate (CWR) is usually several orders of magnitude higher than the critical cooling rate (CCR) [32]. Though the addition of CPAs can significantly decrease the CCR/CWR, it is still challenging to achieve CWR using existing technology. Secondly, traditional permeable CPAs, commonly including glycerol [33], and dimethyl sulfoxide (DMSO) [34], are toxic to biomaterials, and even fatal at high concentrations because CPAs can cause irreversible damage to proteins and cellular structures [35]. In recent years, significant progress has been made in non-toxic and biocompatible bioinspired materials [36,37]. Thirdly, for large and irregular tissues or organs, the temperature distribution is not uniform during the cooling/warming process, leading to the temperature gradient and thermal stress [38], eventually causing mechanical damage to biomaterials. Therefore, no matter whether freezing or vitrification preservation has difficult technical barriers to overcome, which limit the application in tissue and organ cryopreservation [36].

Based on the above introduction of biomaterial cryopreservation, the formation of undesired ice crystals is the greatest challenge of cryopreservation, which is the dominant factor affecting the survival of biomaterials [20]. To improve the efficiency of cryopreservation, ice control strategies are urgently needed to reduce ice damage. To date, many types of CPAs [21,39], antifreeze proteins (AFPs) [40–42], bioinspired materials [7,36,43], and physical field technologies [44] have been utilized to inhibit ice formation, providing a revolutionary improvement in cryopreservation. At the same time, a thought-provoking question arises, that is, how do these specific ice control strategies affect ice formation? To answer it, we have analyzed the basic theory of ice formation and extracted the key affecting factors. Specifically, ice formation mainly consists of nucleation, growth, and recrystallization [45] (Fig. 2). Ice nucleation, the initial and crucial step of freezing [46], refers to the process in which several molecules become arranged in a pattern characteristic of a crystalline solid, forming a nucleus. Ice nucleation is mainly affected by solution melting temperature, ice-liquid interfacial tension, shape factor, and kinetic prefactor. After nucleation, driven by the decrease in free energy, additional water molecules begin to deposit upon the nucleus and form large ice crystals [47]. The key factors affecting ice growth are solution

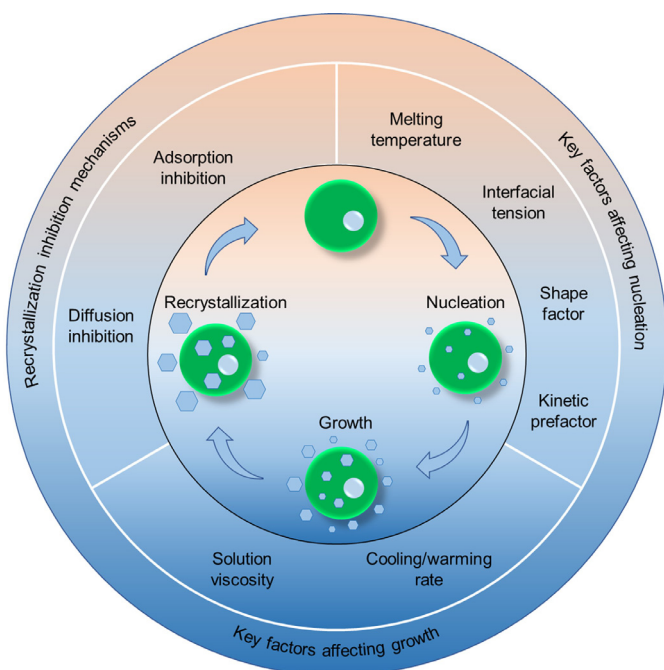


**Fig. 2.** Process of ice formation and an overview of key factors and inhibition mechanisms related to nucleation, growth and recrystallization.

viscosity and cooling/warming rate. Ice recrystallization usually occurs during the warming process, where ice crystals grow larger at the expense of smaller ice crystals, resulting in an overall reduction in free energy [48]. Ice recrystallization can also be regulated by adsorption and diffusion mechanisms. After clarifying the key affecting factors of each process, the link between ice formation mechanisms and existing ice control strategies is established and it has vital guiding significance for efficient cryopreservation.

In this review, we focus on the mechanisms of ice control strategies affecting ice formation and the corresponding applications to biomaterial cryopreservation. We will introduce ice nucleation, growth, and recrystallization in sections 2~4, respectively. In each section, we first introduce the basic theory of each process and construct the essential theoretical framework for readers. Secondly, the key affecting factors are carried out and the specific ice control strategies how to regulate ice formation are analyzed. Moreover, the corresponding research methods and cryopreservation applications of each process are summarized. This review ends with the summary and outlook in section 5. We hope that this study will provide some inspiring insights into efficient cryopreservation.

## 2. Ice nucleation

### 2.1. Classical nucleation theory

Nucleation, a ubiquitous phenomenon in nature, has gained great attention in many aspects of science, from global climate to bioscience. Nucleation is the initial and crucial process of crystal formation [25,46]. Whether crystal phases can form is dominated by the nucleation process. Hence, controlling ice nucleation is critical for cryopreservation. However, despite the great significance of nucleation, the underlying mechanism of ice nucleation are still unclear, owing to the small time scale ( $\sim 10^{-9}$  s) and length scale ( $\sim 10^{-9}$  m) [46]. Currently, the most common theoretical model used to elucidate the nucleation process is the so-called classical nucleation theory (CNT), which was formulated nearly a century ago by Gibbs [49], Volmer and Weber [50], Becker and Döring [51],

and Frenkel [52] et al. Based on CNT, ice nucleation can be well quantified by parameters such as the critical nucleus radius, nucleation barrier, and nucleation rate. The basic framework of CNT will be elaborated on in this section.

In supercooled liquid, due to thermal vibration, the statistical fluctuation of molecules can lead to the spontaneous formation of ordered solid clusters, called ice nuclei. The size of a nucleus fluctuates as free liquid water molecules deposit upon or escape from the nucleus. In general, the thermodynamic driving force for nucleation is the reduction of system-free energy. Due to the chemical potential of the liquid phase  $\mu_l$  being higher than the crystalline phase  $\mu_c$ , the volume free energy  $\Delta G_v$  gradually decreases during the nucleation process, which can be described as [53]:

$$\Delta G_v = \frac{4\pi r^3}{3\nu_c} (\mu_c - \mu_l) \quad (1)$$

where  $r$  refers to the radius of the ice nucleus and  $\nu_c$  is the volume of a molecule in the crystalline phase. The chemical potential change  $\Delta\mu = \mu_c - \mu_l$  is determined by the thermodynamic driving force, which is primarily contributed by supercooling  $\Delta T$ :

$$\Delta\mu \approx -\frac{\Delta H_m}{T_m} \Delta T \quad (2)$$

where  $\Delta H_m$  is the melting fusion of ice,  $\Delta T$  is the difference between melting temperature  $T_m$  and current temperature  $T$ , that is,  $\Delta T = T_m - T$ . Simultaneously, the formation of the nucleus will lead to an increase in surface area. Owing to the interfacial tension at the ice-liquid interface, the surface free energy  $\Delta G_s$  increases, which is unfavorable to nucleation. Thus, the overall free energy change  $\Delta G_{hom}$  is regulated by the competition between the decreasing volume free energy and the increasing surface free energy:

$$\Delta G_{hom} = \Delta G_s + \Delta G_v = 4\pi r^2 \gamma_{lc} + \frac{4\pi r^3}{3\nu_c} \Delta\mu \quad (3)$$

where  $\gamma_{lc}$  is the interfacial tension between liquid and crystal. The relationship between the overall free energy change and nucleus size is shown in Fig. 3. Obviously, there exists a maximum  $\Delta G_{hom}^*$  at  $r = r_c$ , where  $\Delta G_{hom}^*$  is the so-called homogeneous nucleation barrier and  $r_c$  denotes the critical size of the ice nucleus. The values of  $\Delta G_{hom}^*$  and  $r_c$  can be calculated by  $d\Delta G_{hom}/dr = 0$ , which are:

$$\Delta G_{hom}^* = \frac{16\pi \gamma_{lc}^3 \nu_c^2}{3(\Delta\mu)^2} \text{ and } r_c = \frac{2\gamma_{lc}\nu_c}{|\Delta\mu|} \quad (4)$$

The nucleation barrier must be overcome to form a stable crystal; that is, the ice nucleus must reach the critical size  $r_c$  to become thermodynamically stable. For sub-critical nuclei  $r < r_c$ , nucleation is dominated by the surface free energy, and the nucleus may continue to grow or annihilate. While for super-critical nuclei  $r > r_c$ , nucleation is dominated by the volume free energy, thus the nucleus will grow to macroscopic dimensions under the driven force of supercooling.

The discussion above is based on the assumption that the probability of forming a critical nucleus is uniform throughout the system, which is called homogeneous nucleation. Generally, nucleation is often promoted by the presence of foreign substances, called heterogeneous nucleation. The presence of foreign substances in contact with the liquid can significantly lower the interfacial free energy and thus reduce free energy barrier  $\Delta G_{het}^*$ , expressed as [54]:

$$\Delta G_{het}^* = \Delta G_{hom}^* f(\theta) \quad (5)$$

where  $f(\theta)$  is the shape factor ( $0 < f(\theta) < 1$ ). The contact angle  $\theta$  can be calculated through Young's equation  $\gamma_{sl} = \gamma_{lc} \cos \theta + \gamma_{sc}$ , where  $\gamma_{sl}$  is the interfacial tension between the substrate and liquid phase and  $\gamma_{sc}$  is the interfacial tension between the substrate and crystal phase.

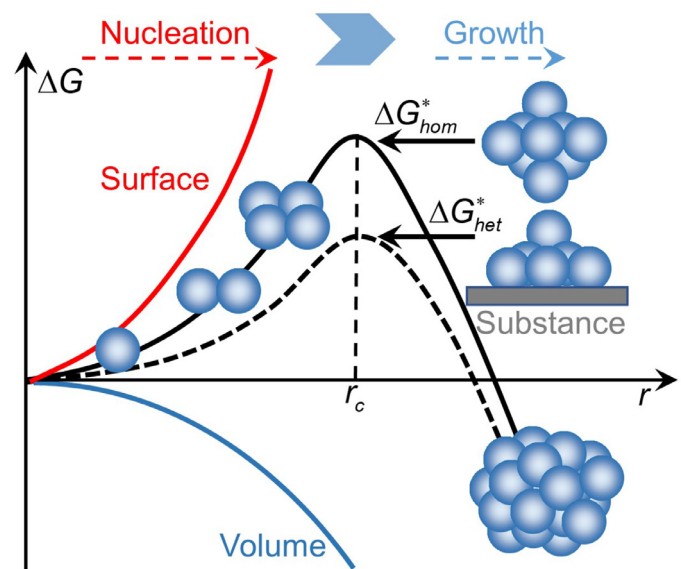


**Fig. 3.** Schematic illustration of classical nucleation theory [46]. The free energy change for homogeneous nucleation (black solid curve) is the sum of the decreasing bulk crystal free energy (blue solid curve) and the increasing surface free energy (red solid curve). For heterogeneous nucleation, nucleation barrier is lowered due to the existence of foreign substances (black dashed curve). (For interpretation of the references to colour in this figure legend, the reader is referred to the web version of this article.)

In practice, numerous ice nuclei form simultaneously in the supercooled liquid, closely associated with phase transitions. Therefore, the nucleation rate is used to quantify the possibility of freezing, which is defined as the number of thermodynamically stable ice nuclei forming per unit volume per unit of time. The nucleation rate  $J$  can be expressed in the form of the following equation:

$$J = J_0 \exp\left(-\frac{\Delta G^*}{k_B T}\right) \quad (6)$$

where  $J_0$  is the prefactor, and  $k_B$  is the Boltzmann constant.

Combining Eqs. (2), (4), (5), and (6), the nucleation rate  $J$  becomes:

$$J = J_0 \exp\left(-\frac{16\pi \gamma_{lc}^3 \nu_c^2 T_m^2}{3k_B T \Delta T^2 \Delta H_m^2} f(\theta)\right) \quad (7)$$

From Eq. (7), there are four key factors affecting the nucleation rate at a certain temperature: melting temperature  $T_m$ , interfacial tension  $\gamma_{lc}$ , shape factor  $f(\theta)$ , and prefactor  $J_0$ , which will be discussed in turn.

## 2.2. Key factors affecting nucleation

### 2.2.1. Melting temperature

Based on Eq. (2), it is obvious that the lower the melting temperature, the less the supercooling, and the smaller the driven force of nucleation, reflected as nucleation inhibition. The use of CPAs in cryopreservation is an embodiment of this approach. Fig. 4A is the typical phase diagram of a CPA solution. The melting temperature and homogeneous nucleation temperature decrease with the increase in CPA concentration within a certain range, following the colligability principle. The most commonly used CPA is DMSO [55], which contains a hydrophilic S=O bond and two hydrophobic methyl groups. As shown in Fig. 4B, the oxygen atom on the S=O bond can form two hydrogen bonds with the water molecules, which is stronger by about 30% than the hydrogen bond between water molecules [56,57]. Polyhydric alcohols, another commonly used CPA, can also form strong hydrogen

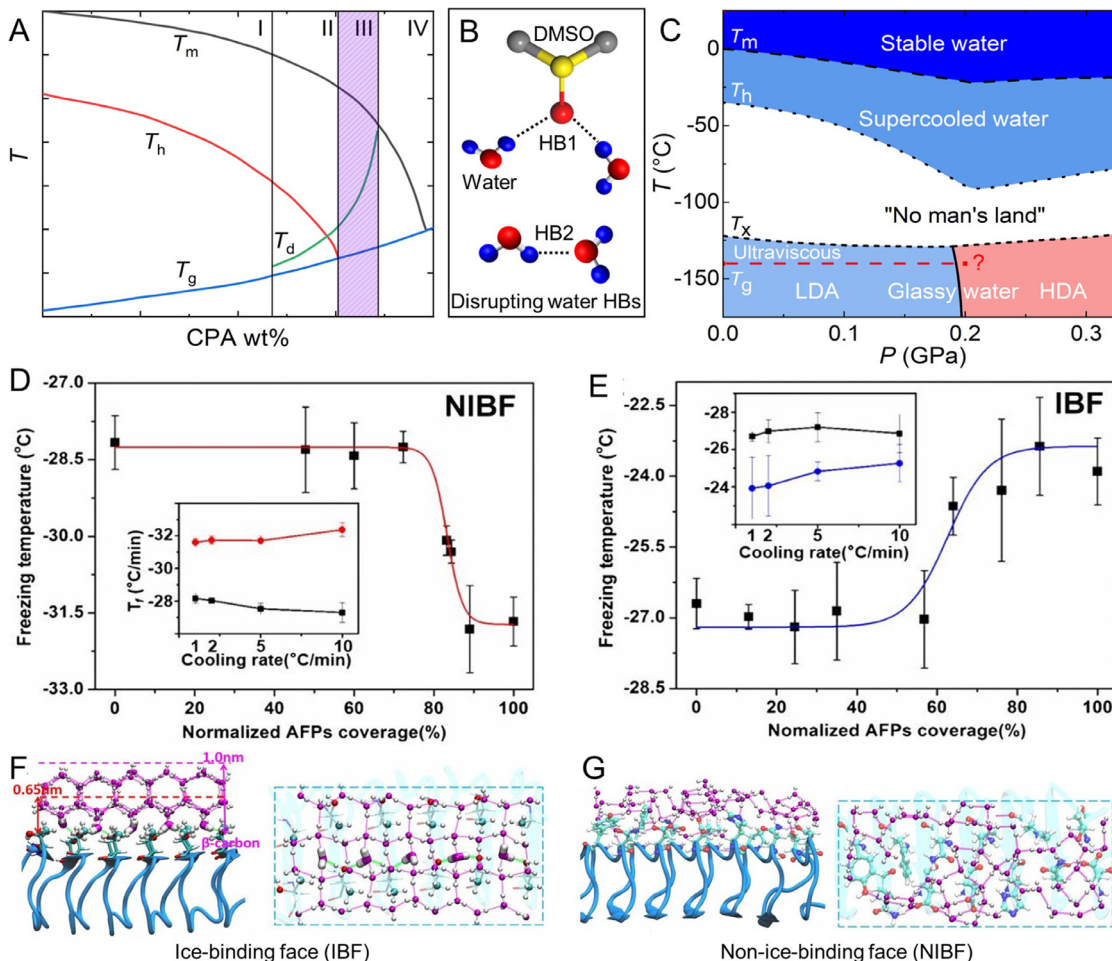


**Fig. 4.** Effect of melting temperature and AFPs on ice nucleation. (A) Phase diagram of a hypothetical CPA solution [218].  $T_m$ : melting temperature.  $T_h$ : homogeneous nucleation temperature.  $T_g$ : glass transition temperature.  $T_d$ : devitrification temperature. The phase diagram for a hypothetical solution of CPA can be divided into four regions. Region I: vitrification is almost impossible due to the extremely high cooling rate required; II: vitrification can be achieved with practical cooling rates but is also prone to crystallization and devitrification; III: vitrification can be achieved with relatively low cooling rates and devitrification is less likely occur; IV: no crystals will form during cooling/warming but the CPA solution is highly toxic to cells. Thus, the purple area corresponds to the optimal CPA concentration in vitrification. (B) Mechanism of DMSO reducing melting temperature. The hydrogen bond formation between DMSO and water (HB1) is stronger than that between water molecules (HB2), disrupting water structure and inhibiting ice formation. (C) Pressure-temperature phase diagram of water [63].  $T_x$ : crystallization temperature; LDA: low-density amorphous; HDA: high-density amorphous. (D-E) Effects of NIBF and IBF on ice freezing temperature [69]. Insets show the ice freezing temperature of the fully covered NIBF and IBF under different cooling rates, respectively, confirming that the NIBF depresses the formation of the stable ice nucleus and the IBF facilitates the formation of the ice nucleus. Black curves represent the freezing temperature of the substrates without AFP. (F-G) Side view and top view of water molecules atop the IBF and NIBF (carbon, nitrogen, and oxygen atoms are represented in cyan, blue, and red spheres, respectively) [69]. The hexagonal ice-like structured hydration layer formed atop the IBF, while the water molecules of the hydration layer atop the NIBF showed a disordered structure. (For interpretation of the references to colour in this figure legend, the reader is referred to the web version of this article.)

bonds with water. Therefore, CPAs can disrupt the hydrogen bond network of liquid water, inhibit the formation of ice nuclei and strengthen the freezing tolerance [58], embodied in the ice-point depression. For example, 25 percent mole fraction of DMSO can depress the melting temperature from 0 °C to -63 °C [59]. To quantitatively analyze the impact of CPA solutions on ice nucleation, Toner et al. [25,60] proposed a theoretical model to calculate the nucleation rate of solution at a certain concentration  $c$ , expressed as:

$$J(c, T) = \Omega(c, T) \exp \left[ -\kappa(c, T) \frac{T_m^5}{T^3 \Delta T^2} \right] \quad (8)$$

where  $\Omega(c, T)$  and  $\kappa(c, T)$  correspond to kinetic and thermodynamic coefficients, respectively. This model has been successfully applied to predict intracellular ice formation and optimize freezing strategies. However, the greatest limitation of the model is that the kinetic and thermodynamic coefficients for certain CPA solutions are not available, because of the combined influence of CPA type,

CPA concentration, temperature, etc. Therefore, the more feasible approach to obtaining the nucleation rate is through freezing experiments or molecular dynamic simulations [61].

Another method to lower the melting temperature is the pressure boost [62]. According to the phase diagram of ice/water (Fig. 4C) [63], with the increase of pressure within 2000 bar, the melting temperature and homogeneous nucleation temperature both decrease. Kanno et al. [62] found that the supercooling of water could even reach -92 °C at 2000 bar, while only -40 °C at normal pressure. Espinosa et al. [64] simulated the water nucleation rate at 1 bar and 2000 bar from the molecular level. They found that at a certain supercooling  $\Delta T$ , the number of molecules required to reach the critical size in compressed water is significantly larger than that at normal pressure, contributing to the decrease in the nucleation rate. However, it is worth mentioning that for large and irregular biomaterials, applying high pressure may cause mechanical damage.

### 2.2.2. Interfacial tension

The ice-liquid interfacial tension  $\gamma_{lc}$  is a key factor influencing nucleation, of which the nucleation barrier is proportional to the third power. Interfacial tension arises from differences between the intermolecular forces at the two phases in contact with each other, mainly affected by the molecular arrangements on both sides of the interface. Hence, there is an instructive direction that tunes the order of liquid water molecules to control nucleation. The closer the structure between liquid and ice phases, the smaller the interfacial tension, and vice versa. The effect of interfacial tension on ice nucleation will be discussed, taking antifreeze proteins and external electric/magnetic fields as examples.

In nature, some plants, insects, and polar fishes can produce AFPs to control ice formation so that they can survive in sub-zero temperatures. However, the intrinsic mechanism of AFPs regulating ice nucleation is unclear, and a consensus has not been reached. Some researchers have found that AFPs can enhance ice nucleation and improve the nucleation temperature [65,66], whereas it has also shown nucleation inhibition effect [67] or no effect [68]. Liu et al. [69] found the Janus effect of AFPs on ice nucleation by selectively investigating the effects of ice-binding face (IBF) and non-ice-binding face (NIBF). Firstly, a hyperactive AFP obtained from a beetle was selectively absorbed on a solid substrate. When IBF was absorbed by polydopamine, the NIBF was exposed to liquid water. It was found that the freezing temperature decreased from -28.0 °C to -31.9 °C (Fig. 4D). On the contrary, when NIBF was absorbed by (3-glycidoxypropyl) methyltrimethoxysilane, the IBF was exposed to liquid water, with the freezing temperature increasing from -27.5 °C to -23.0 °C (Fig. 4E). The results revealed that IBF promoted ice nucleation whereas NIBF inhibited it. Furthermore, molecular dynamic simulation demonstrated the mechanism more intuitively. Due to the regular arrangement of hydrophobic methyl groups and hydrophilic hydroxyl groups, IBF can regulate the liquid water molecules into a hexagonal ice-like structured hydration layer, leading to a decrease in ice-water interfacial tension (Fig. 4F). By contrast, NIBF can regulate the liquid water molecules into a more disordered structure due to the irregular arrangement of hydrophobic/hydrophilic groups and the existence of bulky hydrophobic groups and charged groups (Fig. 4G). Briefly, the ice-like pre-ordered water structure will enhance nucleation and the disordered structure will inhibit nucleation [43].

External electric/magnetic fields can also affect the molecule arrangement of liquid water. For the electrostatic field, it has long been known its application promotes the nucleation process [70,71]. Yan et al. [71] probed the effect of electrostatic field on ice nucleation through molecular dynamics simulation. The orientation of water molecules is random in bulk water initially. Differently, the water molecules are polarized and reorientated along the field after applying an electrostatic field, exhibiting a structure similar to that of cubic ice. Therefore, nucleation is promoted due to pre-ordered water induced by an external static field.

However, for alternating electric or oscillating magnetic fields, the effects are different. The alternating electric field can inhibit ice nucleation, ascribed to the interaction between dipolar water molecules and the electric field. It is equivalent to exerting torque on water molecules, breaking hydrogen bonds, and inhibiting the aggregation of water molecules, as shown in Fig. 5A. The oscillating magnetic field can also affect the movement state of water molecules by orienting, vibrating, and spinning [72], decreasing the formation probability of crystal lattice, as shown in Fig. 5B. Thus, external alternating fields increase the freezing tolerance, increase the nucleation energy barrier, and suppress ice nucleation. Therefore, external physical fields can regulate the spatial configuration of water molecules to control ice nucleation.

### 2.2.3. Shape factor

The main factors affecting  $f(\theta)$  are the contact angle, shape [73,74], and size [75] of the substrate. As shown in Fig. 5C, when the size of foreign substrate  $l$  is large enough ( $l > 2r_c \sin \theta$ ), the contact angle and  $f(\theta)$  remain unchanged:

$$f(\theta) = \frac{(1 - \cos \theta)^2 (2 + \cos \theta)}{4} \quad (9)$$

When  $l < 2r_c \sin \theta$ , to minimize the overall free energy of the system, the geometric angle  $\varphi$  at the edge of substrate increases to  $\sin^{-1}(l/2r_c)$ , causing a higher nucleation barrier. Experimentally, Bai et al. [76] probed the existence of critical nucleus sizes for ice nucleation with a series of graphene oxide (GO) nanosheets. They measured the mean ice nucleation temperatures  $T_{IN}$  of water droplets containing GOs of different sizes, finding an abrupt temperature change at  $|l\Delta T| \approx 200$  nm K. Here,  $l$  is the average lateral size of GOs, and  $\Delta T = T_m - T_{IN}$ . When  $|l\Delta T| < 200$  nm K, ice nucleation occurs on the water-substrate interface and is influenced by the presence of GOs. But when  $|l\Delta T| > 200$  nm K,  $T_{IN}$  is almost independent of the value of  $|l\Delta T|$ . It is inspiring that the critical nucleus size  $r_c$  is approximately equal to  $r_c \approx 100/\Delta T$  nm, consistent with CNT. Under the size effect, the nucleation barrier is changed with  $l$  as shown in Fig. 5C, affecting the nucleation rate.

One typical example is the different functions between AFPs and ice-nucleation proteins (INPs) [77,78]. It has been proved that these two kinds of proteins have similar repeat units but totally different effects on nucleation. INPs can significantly initiate ice nucleation at high subzero temperatures to prevent deep subcooling while AFPs do not. The underlying mechanism lies in the different sizes of AFPs and INPs (AFPs are nearly 1~10 nm, while INPs are 10~100 nm). Qiu et al. [79] elucidated the effect of length on the nucleating efficiency through molecular dynamics simulation. They got the same results as Bai et al. [76], indicating that longer molecules promote nucleation more efficiently. Based on this, many freeze-tolerant animals utilized INPs against low temperatures in nature, as INPs can induce ice nucleation and trigger extracellular ice formation at high sub-zero temperatures to avoid fatal intracellular ice, minimizing the cryoinjury [80].

### 2.2.4. Kinetic prefactor

Though the discussion above is from the view of thermodynamics, the effect of kinetics on the nucleation rate can not be ignored. In fact, the conclusive expression for the prefactor is still an open question, and there are some models [81–86] that described it. Generally, the prefactor  $J_0$  is usually written within CNT as [87,88]:

$$J_0 = \rho_s Z A \quad (10)$$

where  $\rho_s$  is the number of possible nucleation sites per unit volume,  $Z$  is the Zeldovich factor [88], and  $A$  is a kinetic factor. The kinetic factor refers to the frequency with which the particles in the liquid phase reach the cluster rearranging themselves in a crystalline fashion, involving the atomic or molecular mobility of the liquid phase. With temperature decreasing, the self-diffusion coefficient of water molecules also decreases. Thus, for supercooled water, the competing trends of  $\Delta G^*$  and  $A$  lead to a maximum in the nucleation rate as depicted in Fig. 5D. When the temperature is lower than the glass transition temperature  $T_g$ , the viscosity of water is extremely high, and the nucleation rate is almost zero, of great benefit for biomaterials cryopreservation. Based on this, we can achieve vitrification more easily by increasing the viscosity of the solution with CPAs. Compared to pure water, the CPA solutions inhibit molecular mobility and increase the glass transition temperature as described in the phase diagram of a hypothetical CPA solution (Fig. 4A), especially in nonpermeable cryoprotectants such as sucrose [89], and trehalose [90].

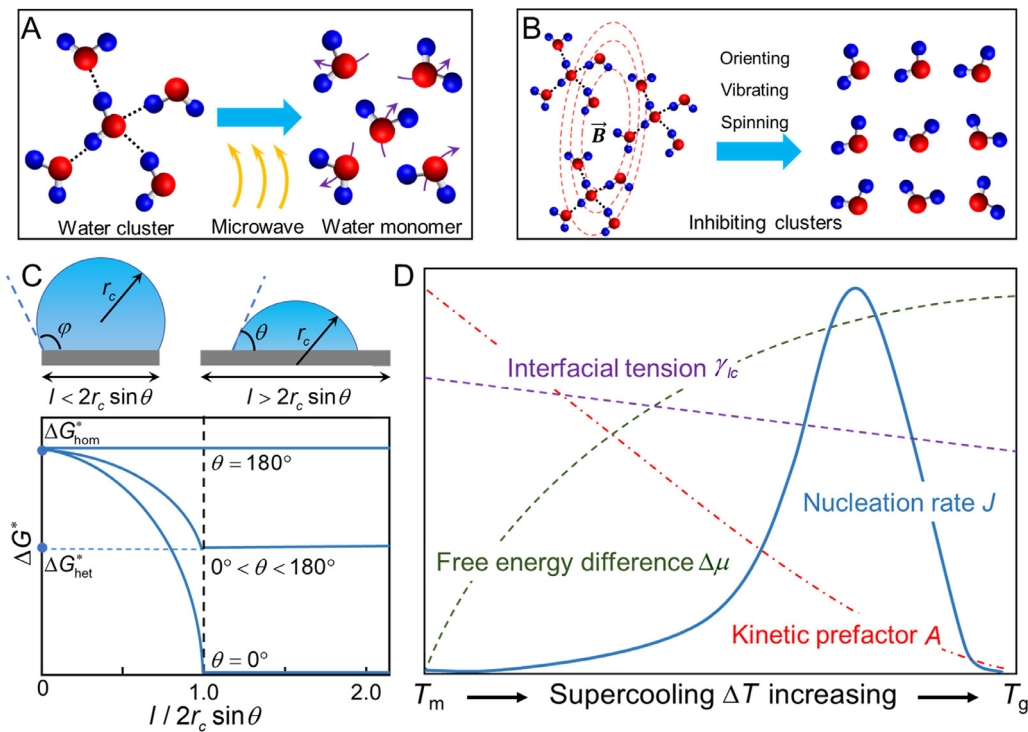


**Fig. 5.** Effect of alternating physical fields, shape factor, and kinetic prefactor on ice nucleation rate. (A) Disturbing effect of microwave irradiation on water clusters [20]. (B) Disturbing effect of oscillating magnetic fields on water clusters by orienting, vibrating, and spinning [20]. (C) Heterogeneous nucleation on a flattened substrate [46]. The contact angle of an ice nucleus on a substrate remains constant when  $l > 2r_c \sin \theta$  and increases as the size of the substrate decreases when  $l < 2r_c \sin \theta$ . The bottom shows the nucleation barrier  $\Delta G^*$  corresponding to the substrate length and contact angle. (D) Illustration of how certain quantities from CNT vary as a function of supercooling  $\Delta T$  in a generic case of diffusion-limited nucleation, characterized by a maximum in the steady-state nucleation rate  $J$  [87].

### 2.3. Measurement of nucleation rates

#### 2.3.1. Optical microscope

Measuring the freezing temperature by optical microscope is the most direct method to analyze ice nucleation activity. As shown in Fig. 6A, numbers of droplets with volume of a few microliters are placed on a hydrophobic glass slide and the freezing temperature of the individual droplets is recorded under the microscope [91,92]. However, due to the existence of glass slides, it is easier to induce heterogeneous nucleation, affecting experimental results. Therefore, to overcome heterogeneous nucleation and study ice nucleation under well-controlled conditions, Liu et al. [67,75] developed a double-oil method. In this approach, the liquid droplet is suspended in two layers of immiscible oil, one of which has a density lower than that of water, and the other has a density higher than that of water (Fig. 6B). The effect of foreign particles can be greatly minimized, and the results are closer to homogeneous nucleation. Due to the stochastic nature of ice nucleation, it is essential to obtain large data sets for the quantitative calculation of nucleation rate  $J$ . Let us consider isothermal nucleation experiments using numerous droplets. If the fraction of frozen droplets is  $f_{ice}(t)$  at time  $t$ , after a time interval  $\Delta t$ , the fraction increases to  $f_{ice}(t + \Delta t)$ .  $J$  can be given as follows [68,93]:

$$J = -\frac{\ln[(1 - f_{ice}(t + \Delta t))/(1 - f_{ice}(t))]}{V \Delta t} \quad (11)$$

where  $V$  is the droplet volume. Therefore, using this experimental method can intuitively analyze the effect of CPAs on ice nucleation, as a guide to cryopreservation.

#### 2.3.2. X-ray scattering

The principle of using X-ray scattering to obtain the nucleation rate is similar to that of optical observation (determining the number of droplets containing ice). Laksmono et al. [94] used a gas

dynamic virtual nozzle to generate a train of microdroplets with uniform diameters, which are subsequently probed by X-rays. They recorded the scattering patterns from each droplet hit by the X-ray pulse and sorted them according to whether they consisted of only diffuse rings indicating scattering from pure liquid water or contained intense and discrete Bragg reflections indicating diffraction from ice crystals [95] (Fig. 6C). Thus, the number of ice-containing droplets  $f_{ice}(t)$  can be calculated, and the nucleation rate at time  $t$  can be obtained using Eq. (11).

#### 2.3.3. Fourier transform infrared spectroscopy

Vibration spectroscopy is a powerful technique to distinguish the physical phase of molecules, which can be used to monitor ice/water. Fourier Transform Infrared (FTIR) spectroscopy is based on the fact that molecules absorb frequencies that are characteristic of their structures. Manka et al. [96] used FTIR spectroscopy to measure the aerosol (containing liquid nanodroplets) spectra and focused on the hydrogen-bonded OH stretch region, 2800~4000 cm<sup>-1</sup> [97]. For supercooled water at 217.4 K, the spectrum exhibited a wide peak at 3370 cm<sup>-1</sup>. But when cooling down to 187.5 K, the spectrum was less symmetric and presented a sharp peak near 3250 cm<sup>-1</sup>, indicating the characteristic of the crystalline state. Therefore, for each experiment, the spectrum lying between the coldest liquid droplets and the fully frozen droplets represents a mixed phase of both (Fig. 6D). By writing the aerosol molar absorptivity  $\varepsilon_a$  as a linear combination of the liquid  $\varepsilon_{a,liq}$  and solid  $\varepsilon_{a,ice}$  absorptivities:

$$\varepsilon_a = f_{ice}\varepsilon_{a,ice} + (1 - f_{ice})\varepsilon_{a,liq} \quad (12)$$

We can estimate the fraction of ice  $f_{ice}$  by fitting Eq. (12) to the intermediate mixed spectra. Furthermore, for two spectra with an interval time  $\Delta t$  at the same temperature, the nucleation rate can be calculated from Eq. (11).

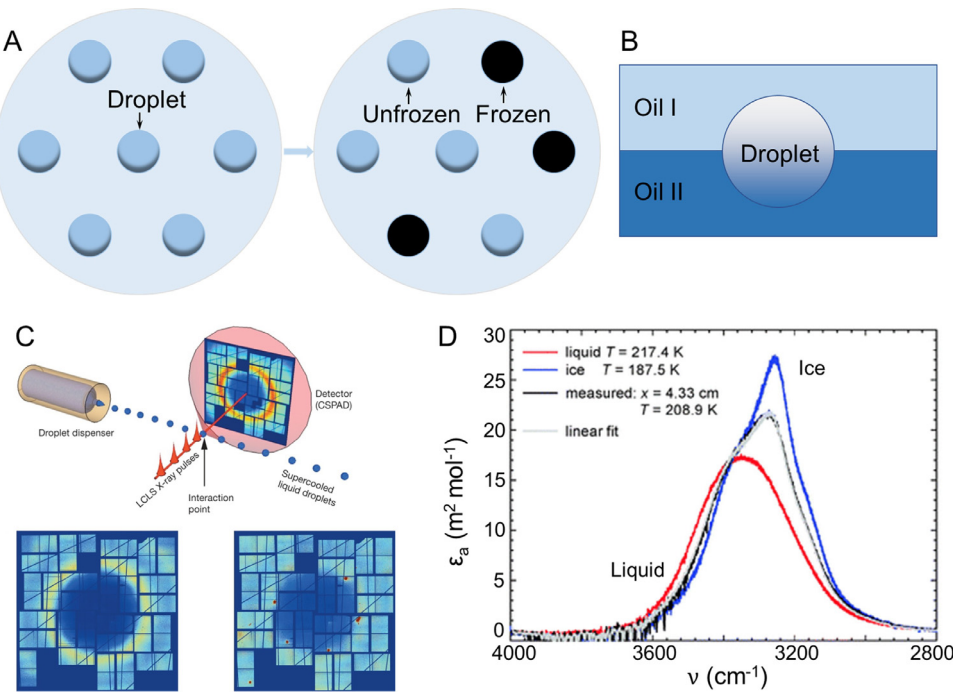


**Fig. 6.** Schematic diagram of the nucleation rate measurement experiment. (A) Optical microscopy image of water microdroplets on the substrate before (left) and after freezing (right). The blue and black droplets mean liquid and frozen phases, respectively. (B) Illustration of the double-oil method [67]. The droplet to be observed is suspended in two oils. Oil I and II represent the density lower or higher than the droplet, respectively. (C) Coherent X-ray scattering from individual micrometer-sized droplets with a single-shot selection scheme [95]. Each diffraction pattern is classified either as a water shot exclusively containing pure liquid scattering characterized by a diffuse water ring (the lower left) or as an ice shot characterized by intense and discrete Bragg peaks superposed on the water scattering ring (the lower right). (D) The mixed-phase FTIR spectrum at 208.9 K can be fit by a linear combination of reference spectra of the liquid water at 217.4 K and ice at 187.5 K [96]. (For interpretation of the references to colour in this figure legend, the reader is referred to the web version of this article.)

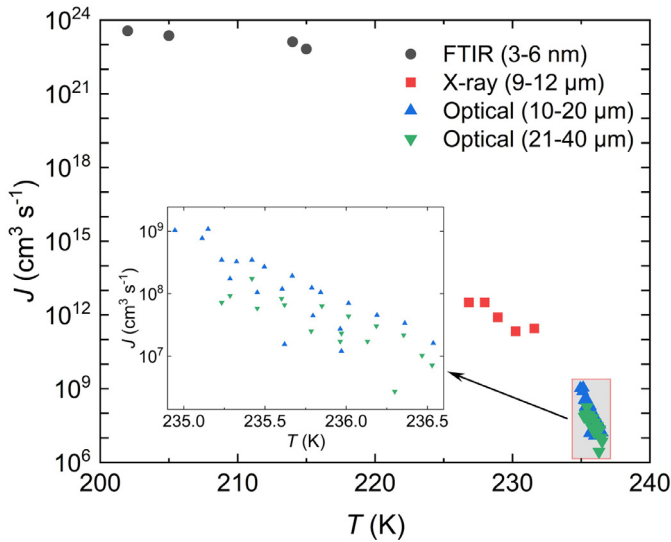


**Fig. 7.** Nucleation rate of diameters ranging from 3 nm~40 μm measured by different experimental methods [94,96,219].

In summary, the above-mentioned experimental methods to estimate nucleation rates are based on the crystallization fraction of lots of microdroplets. Once a nucleus forms in a droplet, it grows rapidly to spread the entire droplet. However, the diameter of droplets that can be observed by optical microscopy is on the scale of μm, while the scale is nm in the FTIR experiment, and the results will be affected by the volume of droplets (as shown in Fig. 7). It has been proposed that freezing may be favored on or close to the surface of micro/nano droplets [98]. If the ice nucleus

forms at the droplet surface and part of the nucleus is in contact with the surrounding air, the free energy of ice nucleus formation is lowered. To describe the freezing of micro/nano droplets, the nucleation rate  $J$  should consider both volume nucleation rate  $J_V$  and surface nucleation rate  $J_S$ :

$$J = J_V + \frac{3}{r} J_S \quad (13)$$

For smaller droplets, which have a much higher surface-to-volume ratio, the surface nucleation plays a more important role during freezing, leading to a higher measured nucleation rate [99]. Moreover, the smaller droplets can reach a higher supercooling, which benefits measuring the nucleation rate at a lower temperature (near 200 K), whereas larger droplets can potentially form more nuclei, resulting in easier crystallization (the temperature range is usually 230~240 K).

#### 2.4. Control strategies for nucleation

In subsection 2.2, four key factors affecting ice nucleation are discussed. Based on this, we systematically summarized the principles of commonly used nucleation control strategies [100] and listed some specific applications in cryopreservation as shown in Table 1. Notably, some issues need to be clarified. Firstly, a specific strategy usually does not affect one factor alone. For instance, the addition of CPAs not only decreases the melting temperature but also increases the solution viscosity, which has multiple inhibitory effects on ice nucleation. Secondly, traditional CPAs such as DMSO and polyhydric alcohols are toxic to cells, reducing the efficiency of cryopreservation despite their excellent ice control ability. One approach is to optimize the loading and unloading procedures of the CPA solution to minimize toxicity [101], and another is to explore novel non-toxic materials to replace them [39]. Thirdly, the

**Table 1**  
Control strategies for nucleation.

Key factors	Control strategies	Details	Biomaterials	Survival	Ref.
Increase $\gamma_{lc}$	CPAs	39% EG + 9% Sorbitol 22% EG + 22%DMSO	Drosophila embryos Islet cells	~60% 95%	[29] [31]
	High pressure	120 MPa	Human RBCs	~70%	[103]
	Alternating electric	2.45 MHz + 5% DMSO	Rat liver cells	62.5%	[104]
	Oscillating magnetic	0.1 mT + 10% DMSO	Stem cells	~90%	[102]
Regulate $f(\theta)$	INPs	10 $\mu\text{g mL}^{-1}$ SNOMAX	Geotrichum candidum	~79%	[105]
Decrease $A$	CPAs	200 mM Galactose	WRL-68	~75%	[106]

EG: ethylene glycol; SNOMAX: ice-nucleating proteins derived from *Pseudomonas syringae*; RBCs: red blood cells; WRL-68: human embryonic liver cells.

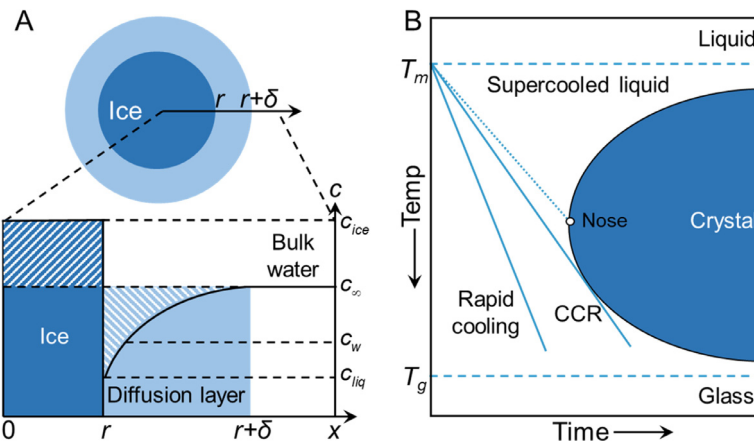


**Fig. 8.** Schematic illustration of ice growth model and temperature-time transformation curve. (A) Ice growth model controlled by diffusion [220]. The upper is the diffusion layer structure near ice crystal, and the bottom is the water concentration as a function of distance. The shaded zone indicates the conservation of water molecules. (B) Temperature-time transformation curve. The edge of the blue zone denotes a fraction of ice crystals and the cooling rate higher than CCR can achieve vitrification without the formation of a certain fraction of ice. (For interpretation of the references to colour in this figure legend, the reader is referred to the web version of this article.)

application of external physical fields requires the optimization of parameters such as frequency and intensity. Kojima et al. [102] investigated the survival rate of rat mesenchymal stem cells after cryopreservation under a magnetic field. When there was a magnetic field intensity of 0.1 mT, the survival rate of cells could reach nearly 90%, higher than that without a magnetic field (76%). However, when the intensity increased to 0.2 mT, the recovered viability of cells decreased to 73%, indicating that the intensity of external fields is a major factor in cryopreservation.

### 3. Ice growth

#### 3.1. Theoretical model

After nucleation, the ice starts to grow under the driven force of reduction of free energy. Several models [25,107–110] based upon classical theories of crystal nucleation and growth have been developed to explain ice formation in aqueous solutions and cells as a function of temperature. Assuming that the ice growth rate is limited by the diffusion of water molecules from the bulk solution to the crystal interface, ice growth can be described by using a non-isothermal diffusion-limited growth model. As shown in Fig. 8A,  $c_{ice}$  is the solid-state water concentration inside the ice crystal,  $c_{liq}$  is the liquid-state water concentration at the crystal interface, and  $c_\infty$  is the liquid-state water concentration far from a crystal. For a spherical ice crystal of radius  $r$ , the flux of water  $F$  from the liquid phase to ice can be described by Fick's first law:

$$F = 4\pi r^2 \bar{D} \frac{dc_w}{dr} \quad (14)$$

where  $\bar{D}$  is the effective diffusion coefficient, which is an average over the concentration range  $c_{liq}$  to  $c_\infty$  and defined as Eq. (18), and

$c_w$  is the liquid-state water concentration. The flux  $F$  can be also rewritten as:

$$F = 4\pi r^2 (c_{ice} - c_{liq}) \frac{dr}{dt} \quad (15)$$

Besides, due to the conservation of water molecules (the shaded zone in Fig. 8A), we can get:

$$\frac{4}{3}\pi r^3 (c_{ice} - c_\infty) = \int_r^{r+\delta} [4\pi x^2 (c_\infty - c_w(x)) dx] \quad (16)$$

where  $\delta$  is the distance from the crystal interface to the bulk water.

Combining Eq. (14)~(16), the ice radius at a time  $t$  of a crystal nucleated at the time  $t_0$  is [111]:

$$r(t : t_0) = \left[ \int_{T(t_0)}^{T(t)} \alpha(T)^2 \bar{D} \left( \frac{dT}{q} \right) \right]^{0.5} \quad (17)$$

where  $\alpha(T)$  is a dimensionless crystal growth parameter, depending on the distribution of  $c_w$ , and  $q$  is the cooling or warming rate. The effective diffusion coefficient is given by:

$$\bar{D} = \frac{1}{c_\infty - c_{liq}} \int_{c_{liq}}^{c_\infty} \frac{k_B T}{6\pi a_0 \eta} dc_w \quad (18)$$

where  $\eta$  is the solution viscosity, and  $a_0$  is the hydrodynamic radius of water.

Assuming spherical ice growth and no overlap between ice crystals, the ice volume  $V_{ice}$  can be calculated at a certain temperature during the cooling or warming process by combining Eq. (8) and (17):

$$V_{ice} = \sum_i^{N(t)} \frac{4\pi}{3} r^3(t : t_i) \quad (19)$$

where  $N(t)$  is the number of nuclei at a given volume  $V_0$ , expressed as:

$$N(t) = \text{int} \left( \int_0^t JV_0 dt \right) \quad (20)$$

Actually, when the ice volume is large enough, overlap inevitably occurs between adjacent ice crystals. In this case, the ice volume fraction  $\chi'$  can be corrected as [112]:

$$\chi' = 1 - \exp(-\chi) \quad (21)$$

where  $\chi = V_{ice}/V_0$ .

### 3.2. Key factors affecting growth

#### 3.2.1. Solution viscosity

Through the above-mentioned theoretical model, growth for a single nucleus mainly depends on the solution viscosity  $\eta$ . The higher the viscosity, the slower the growth rate. As discussed in subsection 2.2, the addition of CPAs and the decrease in temperature can increase the solution viscosity by limiting the mobility of water molecules. CPA molecules can form stronger hydrogen bonds with water, resulting in the retardation of ice growth. Xu et al. [113] investigated the ice crystal growth rate of three kinds of CPAs (DMSO, sucrose, and trehalose) via a high-speed camera. They quantitatively studied the ice crystal growth rate under several critical impact factors such as concentrations of CPAs and cooling rates. As a result, with a cooling rate of  $20^\circ\text{C min}^{-1}$ , the ice growth rate of DMSO solution decreased from  $108.39 \mu\text{m s}^{-1}$  to  $26.05 \mu\text{m s}^{-1}$  when solute concentration increased from 5% to 30%wt. Therefore, high viscosity solution can inhibit ice growth remarkably, forming tiny crystals [30] and lowering the ice damage to cryopreserved cells.

#### 3.2.2. Cooling/warming rate

Cryopreservation can be divided into three processes: cooling, storage, and warming. The cooling rate is a key factor affecting the ice volume crystallized during the cooling process. The cooling rate required to avoid a given volume fraction crystallized  $\chi'$  in a time  $t$  can be estimated by Eq. (21), which is determined by both the nucleation and growth rates. The constructed "C" shape time-temperature for a given volume fraction crystallized is called T-T-T (time-temperature-transformation) curve [60] (Fig. 8B). The nose in a T-T-T curve corresponds to the least time for the given volume fraction  $\chi'$ . This results from a competition between the nucleation rate and the growth rate. The driving force for nucleation increases with decreasing temperature, whereas growth, determined by atomic mobility, decreases with decreasing temperature. When the cooling rate is lower than that represented by the dotted line in Fig. 8B, ice nucleation is the rate control step of ice formation and the nucleation rate increases with the decreased temperature. In contrast, when the cooling rate is higher than that represented by the dotted line, ice growth is the rate control step. Furthermore, when the temperature-time curve continues to increase to be tangent to the C-shaped curve, the cooling rate reaches the CCR. There will not form a certain ice fraction  $\chi'$  during the cooling process if the cooling rate is higher than CCR. Therefore, using rapid cooling methods is easier to achieve vitrification of biomaterials. To date, some advanced approaches have been utilized to improve cooling rates and ensure higher survival rates of cells, which will be introduced below.

The effect of the warming rate is similar to that of the cooling rate. However, the warming process is more challenging, because there is not only the formation and growth of new nuclei but also the growth of nuclei generated during cooling. Therefore, the CWR is usually several orders of magnitude higher than the CCR [32] and often harder to implement.

**Table 2**  
Control strategies for ice growth.

Key factors	Control strategies	Biomaterials	Survival	Ref.
Rapid cooling	Liquid helium	Stem cells	93%	[123]
	Microdroplets	3T3 cells	84%	[124]
	Picodroplets	3T3 cells	86.5%	[125]
	Cryomesh	Islet cells	95%	[31]
Rapid warming	MIH	Stem cells	82%	[129]
		Porcine arteries	/	[126]
		Rat kidney	/	[11]
		Rat heart	/	[28]
PIH		Zebrafish embryos	/	[127]
		HUVECs	>70%	[130]
		HDFCs	94.8%	[131]
	Joule heating	Adherent cells	~60%	[128]

MIH: magnetic induction heating; PIH: photic induction heating; HUVECs: human umbilical vein endothelial cells; HDFCs: human dermal fibroblast cells.

### 3.3. Measurement of growth rates

#### 3.3.1. Optical microscope

Quantifying the ice growth rate of CPA solutions or intracellular ice via an optical microscope has been extensively used [30,114–116]. The ice crystal is characterized by the darkening of the observation zone, and the image data is captured by a high-speed camera. Then the movement of ice crystals edges can be analyzed using continuous images, and thus the ice growth rate. Besides, to make the measurement results more accurate, the edge detection [113] or gray-level variation detection [117] algorithm can be utilized to process images.

#### 3.3.2. Differential scanning calorimetry

Differential scanning calorimetry (DSC) is a thermal analytical technique in which the heat flow into or out of a sample is measured as a function of temperature [118]. Thus, DSC can be used to monitor the mass of ice formation during the cooling process. The DSC signal (thermal power  $W$ ) is the amount of heat released per unit of temperature. The thermal power is integrated to obtain the mass of ice  $\Delta m$  that forms from  $T_1$  to  $T_2$  ( $T_1 < T_2$ ) during crystallization. Therefore,  $\Delta m$  can be expressed as [119]:

$$\Delta m = \int_{T_1}^{T_2} \frac{W(T)}{\Delta H_m(T)q} dT \quad (22)$$

where  $q$  is the cooling rate, and  $\Delta H_m(T)$  is the ice melting enthalpy at temperature  $T$ . DSC can also be used to monitor phase transitions and predict the CCR of the CPA solution. For example, Sutton [120] utilized it to construct T-T-T curves [121] or continuous cooling curves [122] of aqueous solutions (Fig. 8B), from which CCR can be estimated.

### 3.4. Control strategies for growth

In this subsection, we mainly introduce some advanced cooling or warming methods used in cryopreservation, summarized in Table 2. To realize a rapid cooling rate, there are three potential directions: lower-temperature cold source, smaller sample volume, and higher heat transfer coefficient. It is well known that liquid helium has a lower boiling temperature than commonly used liquid nitrogen and can achieve a higher cooling rate. Dou et al. [123] investigated the vitrification efficiency of human bone-derived mesenchymal stem cells under liquid helium (Fig. 9A). As a result, there was a significant difference in immediate cell viability between cells vitrified in liquid helium ( $93.0 \pm 0.7\%$ ) and liquid nitrogen ( $82.6 \pm 4.1\%$ ). The second method is to reduce the volume of cryopreserved samples. Shi et al. [124] developed a non-contact vitrification device and uniform cell-laden microdroplets with volume of a few microliters were generated by a high-throughput

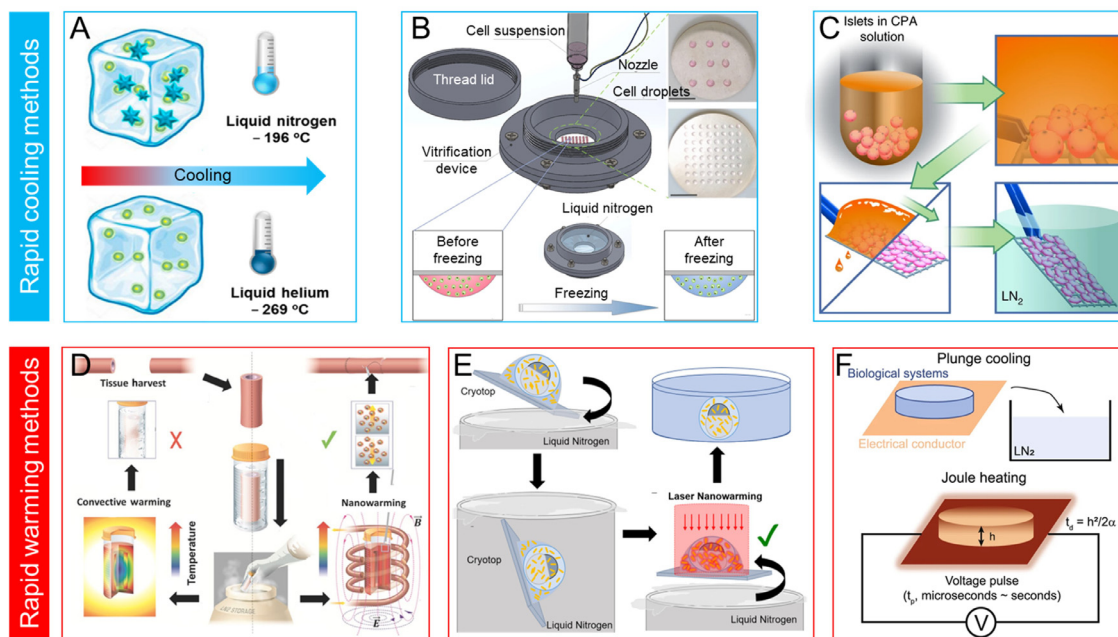


**Fig. 9.** Summary of rapid cooling and warming methods. (A) Illustration for cell vitrification using liquid nitrogen or liquid helium as cryogens [123]. Ice crystals formed by using liquid nitrogen while not by using liquid helium. (B) Schematic of the cell printing-based non-contact vitrification device [124]. The microdroplets containing cells are prepared by the printing nozzle. Scale bars: 10 mm. (C) Schematic of cryomesh vitrification method. After CPA loading, islets in suspension were transferred to the cryomesh, and excessive CPA solution was removed before being plunged into liquid nitrogen [31]. (D) Schematic illustrating tissue vitrification, convective warming, and nanowarming. Nanowarming in an alternating magnetic field, an inductive radiofrequency coil that simulated nanoparticles heating [126]. (E) Schematic of zebrafish embryo cryopreservation and laser nanowarming. Laser nanowarming yields rapid and uniform warming inside the embryo to outrun any ice formation [127]. (F) Schematic of biological systems cryopreservation using plunge cooling and joule heating [128].

cell printer (Fig. 9B). The device can improve the cooling rate to  $1146\text{ }^{\circ}\text{C min}^{-1}$  and achieve an 84% survival rate of 3T3 cells. On this basis, Akiyama et al. [125] developed a super flash freezing system to realize the cryoprotectant-free cryopreservation of mammalian cells. In this way, the droplet volume can decrease to 40 picoliters and the corresponding cooling rate reaches  $2.22 \times 10^6\text{ }^{\circ}\text{C min}^{-1}$ . The third method is to reduce the heat transfer resistance between liquid nitrogen and cells. Zhan et al. [29] developed a cryomesh system, consisting of a nylon mesh attached to a plastic handle (Fig. 9C). The cells will be immobilized in the pores of the cryomesh and the additional CPA solution can be removed by wicking, improving the heat transfer efficiency and increasing the cooling rate to  $5.4 \times 10^4\text{ }^{\circ}\text{C min}^{-1}$ .

The above-mentioned method can also be applied to increase the warming rate. Moreover, there are three alternative methods to achieve uniform rapid rewarming: magnetic induction heating, photic induction heating, and joule heating. Manuchehrabadi et al. [126] successfully achieved vitrification of 50 mL porcine arteries by magnetic nanowarming (Fig. 9D). They synthesized silica-coated iron-oxide nanoparticles, which possess excellent biocompatibility, stability, dispersibility, and high magnetothermal effect. After applying the external magnetic field, the nanoparticles can rapidly convert magnetic energy into thermal energy, achieving rapid and uniform rewarming. Moreover, the uniform distribution of nanoparticles can also lower the thermal stress in tissues and organs, improving the efficiency of vitrification. The second method is laser nanowarming, harnessing the ability of nanoparticles to convert photic energy into thermal energy. Khosla et al. [127] addressed the cryopreservation of zebrafish embryos by using gold nanorods to assist laser nanowarming (Fig. 9E). As a result, the survival rate of embryos by nanowarming is 31% after 1 h while 0% by convective warming. Recently, Bischof and co-workers [128] reported a rapid rewarming method using joule heating as shown in (Fig. 9F). The biological systems were in contact with the electrical conductor. For rewarming, the electrical conductor

was connected to a voltage pulse generator and generated heat via joule heating, which can achieve a warming rate of  $6.7 \times 10^8\text{ }^{\circ}\text{C min}^{-1}$  for cells. In conclusion, rapid cooling and warming methods can inhibit ice growth, making cryopreservation of tissues and organs possible.

#### 4. Ice recrystallization

##### 4.1. Phenomenon of recrystallization

After ice nucleation and growth, many ice crystals of different sizes form. During the warming process, the recrystallization of ice in liquid solution is believed to occur through the Ostwald ripening process. The process is a thermodynamically driven, in which large ice crystals grow at the expense of small ones [132,133]. Ideally, if the ice crystals are the same size as each other, local equilibrium requires their intersection angles at the triple junctions to be about 120°, as depicted in Fig. 10A [134]. However, ice crystals are usually different in size and curvature. For a large crystal, there are small ice crystals around it. Large crystals have more concave boundaries and have a lower amount of surface energy, while small crystals have more convex boundaries [134] (Fig. 10B). Kelvin's equation describes the relationship between the boundary curvature and the chemical potential [135]:

$$\mu = \mu_0 + \frac{2\gamma_{lc}v_c}{r} \quad (23)$$

where  $\mu_0$  is the chemical potential of an atom at a flat interface,  $\gamma_{lc}$  is the interfacial tension,  $v_c$  is the molar volume of crystalline phase, and  $r$  is the radius of the particle. The chemical potential of an ideal solution can also be expressed as a function of the solute concentration  $C_{eq}$  when liquid and solid phases are in equilibrium:

$$\mu = k_B T \ln(C_{eq}) \quad (24)$$

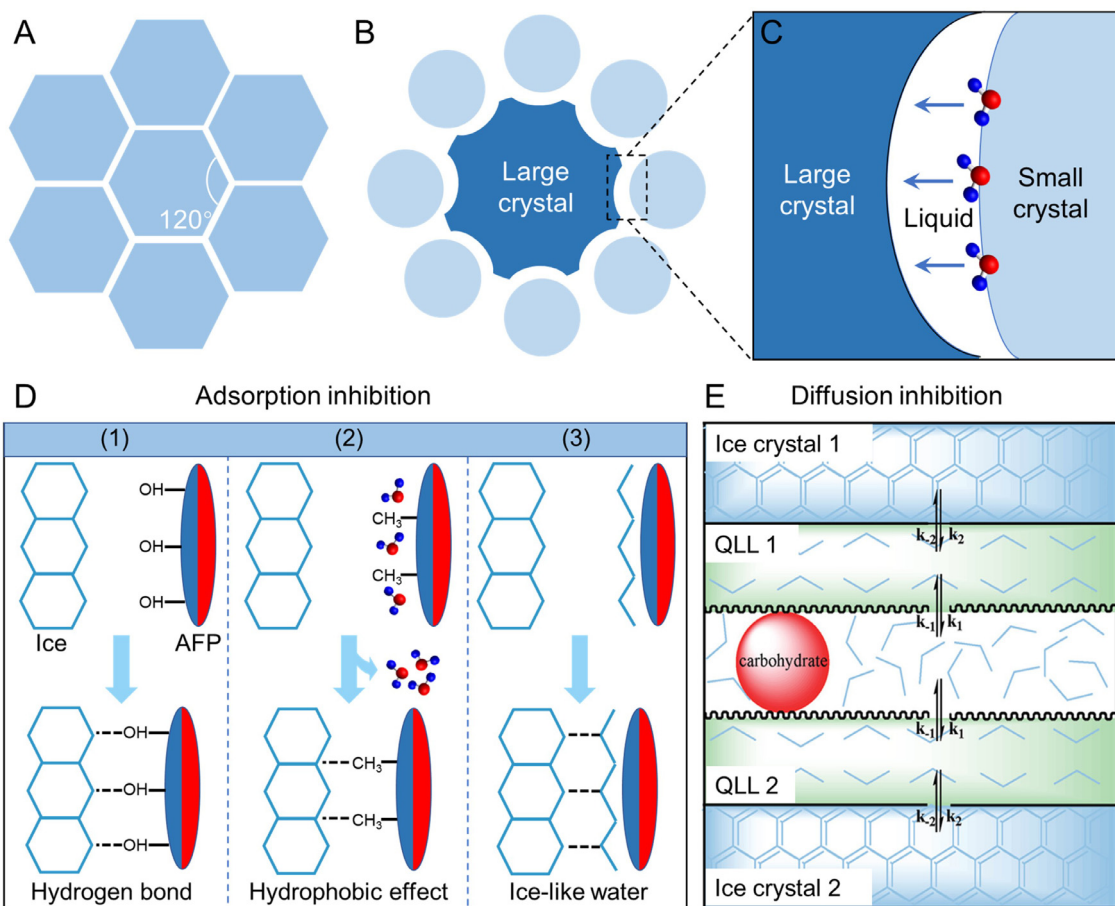


**Fig. 10.** Ice recrystallization phenomenon and inhibition mechanisms. (A) The intersection angles at the triple junctions are 120° if the ice crystals are the same size. (B) Large crystals tend to have concave boundaries and small crystals tend to be convex. (C) Schematic of boundary migration of adjacent ice crystals. The arrows indicate the moving direction of water molecules [134]. (D) Three proposed adsorption inhibition mechanisms for AFPs binding to ice. The blue and red faces represent the IBF and NIBF of AFPs, respectively. (1) Hydrogen bonding hypothesis. The hydroxyl spacing on IBF matches the ice lattice structure and the hydroxyl groups form hydrogen bonds with water molecules in the ice. (2) Hydrophobic effect. Solvent water molecules around hydrophobic groups on the IBF are released into the solution upon the AFP binding to ice. (3) Ice-like water hypothesis. The water molecules around IBF exhibit an ice-like structure, bind to the ice surface through hydrogen bonds and eventually form ice. (E) Diffusion inhibition mechanism [144]. Carbohydrate residues at the QLL-bulk water interface between two adjacent ice crystals disorder the water molecules, which inhibits their mobility. (For interpretation of the references to colour in this figure legend, the reader is referred to the web version of this article.)

Combining Eq. (23) and (24) the following equation can be obtained [136]:

$$C_{eq}(r) = C_{eq}(\infty) \exp\left(\frac{2\gamma_c v_c}{k_B T r}\right) \quad (25)$$

where  $C_{eq}(\infty)$  is the equilibrium solute concentration at a flat interface. Thus, the equilibrium solute concentration is lower around large crystals than that around small crystals. Inferring from Fick's first law of diffusion, atoms will migrate from regions of high to low curvature, resulting in ice crystals with concave boundaries (larger crystals) growing larger while those with convex boundaries (smaller crystals) decreasing in size (Fig. 10C). Therefore, the driving force of Ostwald ripening arises from the reduction in crystal boundary curvature, leading to an overall reduction in the system energy [137].

To quantitatively analyze the ice recrystallization process, there are several derivations of theoretical models [136]. Lifshitz et al. [138] and Wagner [139] developed a method for treating an ensemble of coarsening particles and made quantitative predictions on the long-time behavior of Ostwald ripening. When the diffusion of water molecules through the liquid phase between ice crystals determines the overall kinetics of ice recrystallization, the temporal increase in the mean crystal radius  $r$  can be described as the theory proposed by Lifshitz, Slyozov and Wagner (known as LSW

theory)[138,139]:

$$r^3(t) - r_0^3 = k_d t \quad (26)$$

where  $r_0$  is the initial mean radius at time  $t = 0$ , and  $k_d$  is the observed rate constant of recrystallization, which depends on solution viscosity, temperature, interfacial tension, etc.

#### 4.2. Mechanisms of recrystallization inhibition

In cryopreservation, ice recrystallization usually occurs during the warming process, resulting in the formation of large ice crystals and fatal cryoinjury to biomaterials, which forces us to investigate the underlying mechanisms [48,133,140–142]. It is worth noting that different ice recrystallization inhibition (IRI) agents correspond to different mechanisms, summarized as adsorption inhibition and diffusion inhibitions. Briefly, adsorption inhibition [143] means that the ice-binding face of IRI agents adsorbs to ice and the non-ice-binding face is exposed to water, preventing liquid water molecules from depositing on ice, and inhibiting the ice growth and recrystallization (Fig. 10D). Diffusion inhibition [144] exhibits IRI activity by altering the structure of bulk water and/or the quasi-liquid layer (QLL, a layer of semi-ordered ice), leading to an increase in disorder (Fig. 10E). Hence, the energy required for the migration of water molecules between adjacent ice crystals is higher, resulting in the inhibition of ice recrystallization.

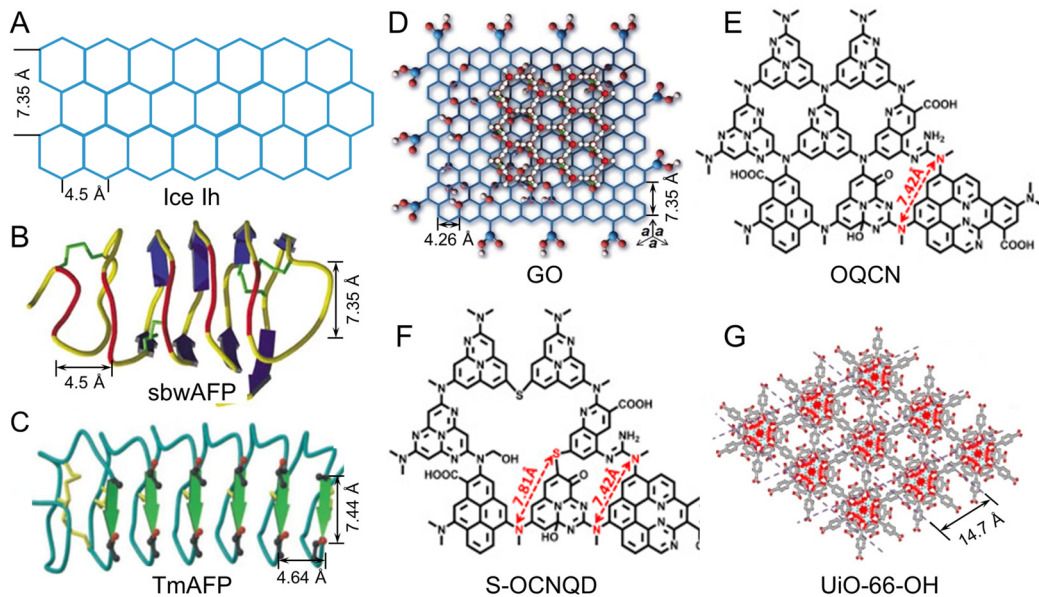


**Fig. 11.** Molecular structures of ice Ih and some IRI agents. (A) Molecular structure of the basal face of ice Ih. The lattice parameters of ice Ih are  $7.35 \times 4.5 \text{ \AA}$ . (B) Molecular structure of recombinant spruce budworm antifreeze protein (sbwAFP) [146]. (C) Molecular structure of *Tenebrio molitor* AFP (TmAFP) [147]. (D-G): Molecular structures of GO [152], OQCN [153], S-OCNQD [154], and UiO-66-OH (one kind of Zr-based MOF) [155], respectively. The feature sizes of the above-mentioned IRI agents match the lattice constants of ice Ih.

#### 4.2.1. Adsorption inhibition

AFPs have shown strong IRI activity in previous studies [140], which is ascribed to their adsorption-inhibition effect [143]. However, AFPs are a complex class of compounds with different structures, making it difficult to deduce the specific mechanisms by which they bind to ice. There are three potential explanations related to key groups of molecular structure [140], upon which IRI agents are based.

**Hydrogen bond.** Based on structure matching between some AFPs and hexagonal ice Ih (detailed information of AFP types and ice Ih can be found in ref [142,143]), hydrogen bonds seem to be the main driving force of ice binding (see (1) in Fig. 10D). The lattice parameters of hexagonal ice are  $7.35 \text{ \AA} \times 4.5 \text{ \AA}$  [145], as shown in Fig. 11A. Graether et al. [146] obtained the structure of antifreeze protein of recombinant spruce budworm through nuclear magnetic resonance experiments. They presented the relative threonine residues positions of the AFP as shown in Fig. 11B, aligning in a grid-like arrangement spaced  $7.35 \text{ \AA}$  and  $4.5 \text{ \AA}$  apart. Liou et al. [147] investigated the structure of the beetle *Tenebrio molitor* AFP, of which the IBF shows a  $\beta$  helix. As shown in Fig. 11C, the average distance between hydroxyls within the  $\beta$ -sheet motif is  $7.44 \text{ \AA}$  and the distance between adjacent threonine residues is  $4.64 \text{ \AA}$ . Similar structures were also found in other ice-binding proteins [148–151]. Such structures well matched to the basal face of the ice, supporting the hydrogen bonding mechanism. Bioinspired by the lattice-matching structure of AFPs, there are many ice-controlling materials have been developed in recent years. GO shows the co-existence of large oxidized and unoxidized graphene regions on the surface of GO [152], where the hydroxy and epoxy groups are located at oxidized regions and the carboxyl groups mainly localized at the periphery of GO (Fig. 11D). The basal plane of GO consists of repeated honeycomb hexagonal carbon rings ( $7.35 \text{ \AA} \times 4.26 \text{ \AA}$ ), offering a suitable reason for its IRI capability. Oxidized quasi-carbon nitride quantum dots (OQCNs) [153] are a derivative of GO (Fig. 11E). The tertiary nitrogen atoms possessing an isolated electron pair can function as the acceptor of a hydrogen bond and the distance between two adjacent tertiary nitrogen atoms is about  $7.42 \text{ \AA}$ , estimated according to bond lengths

and angles. Sulphur-doped oxidized quasi-carbon nitride quantum dots (S-OCNQDs) [154] are similar to OQCNs, where partial tertiary nitrogen atoms are substituted by sulphur atoms (Fig. 11F), resulting in the distance between nitrogen and sulphur atoms being changed to  $7.81 \text{ \AA}$ . Zirconium-based metal-organic framework (Zr-based MOF) nanoparticles [155] are also utilized for IRI, and the periodic arrangement of organic linkers on the surface of MOF nanoparticles provides a precise spacing of hydrogen donors to recognize and matches the ice crystal planes (Fig. 11G).

**Hydrophobic effect.** The second mechanism suggests that the hydrophobic effect between hydrophobic groups and ice dominates the adsorption process [156,157] and affects IRI (see (2) in Fig. 10D). The Gibbs free energy change  $\Delta G = \Delta H - T\Delta S$  during adsorption is affected by the enthalpy change  $\Delta H$  and entropy change  $\Delta S$ . The driving force of the hydrogen bond mechanism mentioned above is enthalpically driven by the formation of hydrogen bonds. By contrast, the hydrophobic effect mechanism is entropically driven [158]. The solvent water around the hydrophobic groups on the IBF might be released into the bulk solution upon the AFP binding to ice, resulting in an entropic gain. Threonine substitution experiments are strong evidence for the hydrophobic effect. Haymet et al. [159] selected winter flounder AFP as experimental subjects, in which threonines were arranged orderly at the ice-binding sites. When several threonines in the middle were replaced by serines, the AFP almost lost all activity, despite serines can potentially form hydrogen bonds just as effectively as threonines. By contrast, replacement by valines only caused little loss of activity, indicating that the methyl group of threonine might be important for ice-binding. According to this mechanism, hydrogen bonds are beneficial but not essential. Based on this, the role of hydrophobic groups in many AFP derivatives and polymers can not be ignored and has been studied in detail [160–162]. Poly(vinyl alcohol) (PVA) is an agent with extremely high IRI activity [163]. The driving force behind PVA binding to ice is widely accepted to be enthalpically driven [164]. However, since PVA is a flexible molecule and can typically be found in a random coil conformation, only 35% of its hydroxyl groups that are hydrogen bonded to the ice surface [165], indicating additional driving forces may

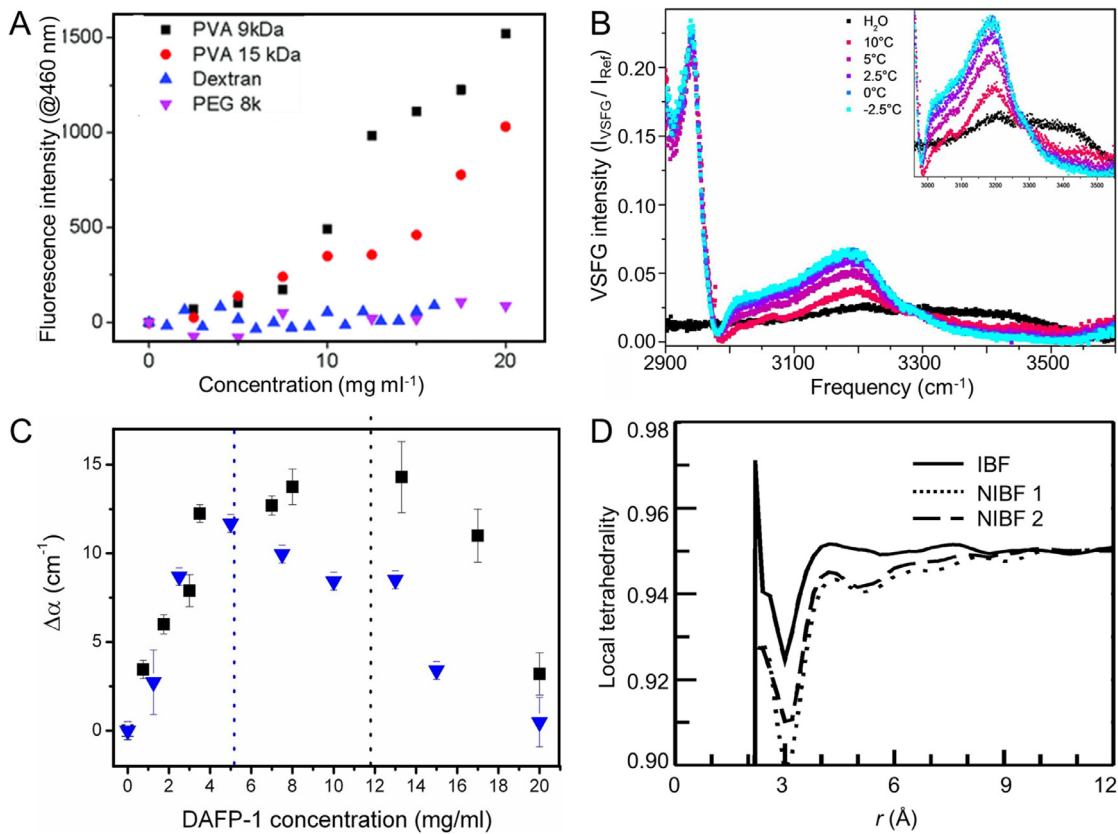


**Fig. 12.** Literature review of adsorption inhibition measurements. (A) Fluorescence of diphenyl hexatriene versus concentration of PVA, Dextran, and PEG [166]. (B) VSFG spectra of a 20- $\mu$ M AFP III at different temperatures [169]. For comparison, the VSFG of the water-air interface is also shown (black). (C) Concentration-dependent terahertz absorption of the beetle Dendroctonus canadensis AFP (DAFP-1) [171]. The results were relative to pure water and integrated between 2.4 and 2.7 THz. Measurements were carried out at  $293.15 \pm 0.5$  K (black data points) and  $278.15 \pm 0.5$  K (blue data points). (D) The local tetrahedral coefficient of solvation water as a function of the distance to the nearest heavy atom of AFP at 250 K [173]. (For interpretation of the references to colour in this figure legend, the reader is referred to the web version of this article.)

contribute to the adsorption of PVA. Bachtiger et al. [165] confirmed that the PVA-ice interaction also benefits from entropic gain through simulation. The first solvation shell of hydrophobic methylene groups contains five water molecules on average in solution, while the number of water molecules decreases and ice molecules correspondingly increases within the solvation shell after the PVA-ice interaction. Therefore, there is an entropic contribution as the solvation shell of methylene is structurally constrained compared to the bulk phase. Deller et al. [166] carried out a dye inclusion assay to explore the underlying mechanism experimentally. An aqueous solution of diphenyl hexatriene, only fluorescing in hydrophobic environments, was prepared and PVA, dextran and poly(ethylene glycol) (PEG) titrated into this solution with vigorous mixing. As a result, in Fig. 12A, the addition of PVA led to a large and significant increase in fluorescence, demonstrating that PVA does indeed form hydrophobic domains.

*Ice-like water around IRI agents.* The third mechanism for the adsorption of AFPs to ice is the ice-like water structure [167,168]. Different from the above-mentioned mechanisms, requesting the direct contact between AFPs and ice crystals, ice-like water forms near the ice-binding sites of AFPs, then binds to ice through hydrogen bonds in this mode (see (3) in Fig. 10D). In other words, it is an indirect binding mechanism. In fact, it is difficult to directly observe the ice-like water around AFPs, requiring spectral experiments or molecular dynamic simulations to confirm. Herein, we present several studies about it briefly. Firstly, vibrational sum-frequency generation (VSFG) spectroscopy is a suitable method to probe the surface between liquids and solids with high selectivity.

The principles of VSFG can be found in ref[77]. Briefly, in an aqueous solution of AFP, there is no sum-frequency signal generated in bulk water due to the symmetry, but a strong signal is generated at the interface between AFP and water. And interestingly, the more ordered the interfacial water structure, the stronger the signal is. Meister et al. [169] used this method to observe the ice-like water of AFP III from an Antarctic eelpout. As shown in Fig. 12B, for pure water, the VSFG spectrum is almost zero at the whole wavenumber range; but the VSFG spectra of a 20- $\mu$ M AFP III solution at different temperatures show a narrow peak at  $3200$  cm<sup>-1</sup>, which is similar to the OH vibration spectrum of ice. Therefore, the results demonstrate the existence of the ice-like water layer at the AFP surface. The ice-like water content will increase slightly with decreasing temperature. Secondly, terahertz spectroscopy was also used to probe the hydration dynamics around AFPs [170,171], as well as the collective water network motions. In principle, the overall terahertz absorption  $\alpha_{total}$  of AFP solution can be described by [172]:

$$\alpha_{total}V_{total} = \alpha_{AFP}V_{AFP} + \alpha_{hydration}V_{hydration} + \alpha_{bulk}V_{bulk} \quad (27)$$

where  $\alpha_{AFP}$ ,  $\alpha_{hydration}$ , and  $\alpha_{bulk}$  are the absorption coefficient of the AFP, the hydration shell, and the bulk water, respectively.  $V_{total}$ ,  $V_{AFP}$ ,  $V_{hydration}$ , and  $V_{bulk}$  are the volume of the total solution, AFP molecules, hydration shell, and bulk water, respectively. Because of  $\alpha_{AFP} < \alpha_{bulk} < \alpha_{hydration}$ , when the AFP concentration is low that the hydration shells do not overlap, the  $\alpha_{total}$  increases with the increase of AFP concentration. But when AFP concentration is high enough, the  $\alpha_{total}$  gradually decreases with the increase of

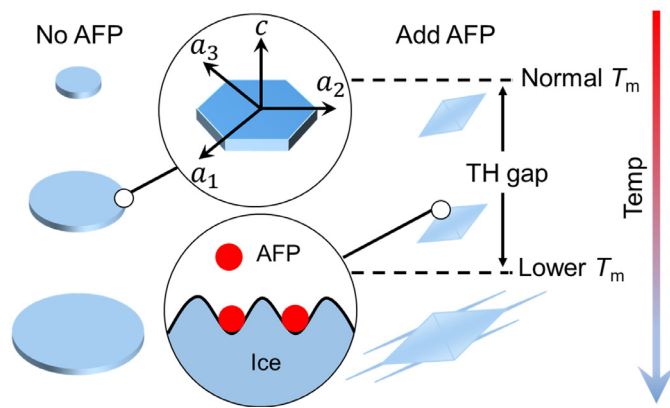


**Fig. 13.** Thermal hysteresis [140]. Ice nucleus grows along the  $a$ -axis uniformly and forms a disk-shaped crystal without AFPs. Due to AFPs (red dots), the growing edges of ice crystal bulge outwards along the  $a$ -axis, and the freezing temperature is lower than the equilibrium freezing temperature. Ice crystal grows uncontrollably along the  $c$ -axis below the freezing point. (For interpretation of the references to colour in this figure legend, the reader is referred to the web version of this article.)

AFP concentration. Therefore, the thickness of the hydration shell can be calculated through the peak of excess terahertz absorption  $\Delta\alpha = \alpha_{\text{total}} - \alpha_{\text{bulk}}$ , because the absorption coefficient of the AFP is much smaller than those of the hydration shell and the bulk water. Meister et al. [171] investigated the terahertz absorbance of a beetle *Dendrodoea canadensis* AFP. As shown in Fig. 12C, when the temperature decreases from 293 to 278 K, a shift of  $c_{\text{max}}$  from 12 to 5 mg mL<sup>-1</sup> is found, indicating an increase in the size of the dynamic hydration shell from 20 to 27 Å. Therefore, the long-range interaction between AFP and water is supposed directly correlated to IRI activity. Compared to spectroscopic methods, molecular dynamic simulations can provide molecular-level insights and indicate that an AFP is capable of ordering water molecules into an ice-like structure. A typical example is the study of winter flounder AFP by Nutt et al. [173]. They analyzed the behavior of water molecules around the IBF and NIBF, including the local tetrahedral coefficient, the mean-square displacement, and the hydrogen bond lifetime. As shown in Fig. 12D, the results indicated that the water structure was ordered (higher local tetrahedral coefficient) around the IBF, with a disordering effect observed around the NIBF. Therefore, the preordered hydration shell around the IBF is involved in the initial recognition and binding of the antifreeze protein to ice.

Based on the adsorption-inhibition mechanism, AFPs bind to the ice surface tightly, leading to thermal hysteresis (TH) [174–176] (Fig. 13). In practice, individual water molecules crystallize into a lattice containing four different axes:  $a_1$ ,  $a_2$ ,  $a_3$  (prism plane), and the  $c$ -axis (basal plane), where ice growth typically occurs along the  $a$ -axis [177]. However, in the presence of AFPs, the adsorption of AFPs to the  $a$ -axis prevents ice growth, and the curvature of the prism plane increases. Therefore, there exists a local freezing temperature depression  $\Delta T$  compared to the normal freezing temperature  $T_m$ , described by Kelvin equation [178]:

$$\Delta T = \frac{\gamma_c T_m v_c}{\Delta H_m} \frac{dS}{dV} \quad (28)$$

where  $dS/dV$  is the derivative of the area of an ice crystal with respect to its volume. Herein, the freezing temperature depression means the rapid growth temperature of ice is lowered, not suppressing the formation of ice nuclei. Within the TH gap, the ice crystal does not increase in size. However, at temperatures below the hysteresis freezing point, the ice crystal will grow uncontrollably along the  $c$ -axis, often at extreme speeds, into long spicules [174,179]. This rapid “burst” growth habit and needle-like ice un-

doubtedly will cause fatal injuries to biomaterials, limiting the application of AFPs in cryopreservation.

#### 4.2.2. Diffusion inhibition

The above discussion is based on adsorption inhibition and exhibits an undesired TH gap. However, some small IRI molecules such as carbohydrates [144] and AFP analogs [180] do not show TH activity in experiments, belonging to diffusion inhibition. The viscosity of the solution is the dominant factor in diffusion inhibition, which can be affected by the hydration or electrostatic interaction of IRI agents.

**Hydration.** IRI ability of small molecules with molecular weight less than 1000 daltons [181] was thought to be correlated to the hydration of their carbohydrate residues. The hydration index is defined as the number of tightly bound water molecules per molar volume of carbohydrate [144]. Since these small molecules do not show an ice-binding surface, they remain in the bulk water-QLL interface during crystallization. The hydration of carbohydrate residues can disrupt the hydrogen bonds between water and disorder the bulk water surrounding the hydration shell, increasing the energy barrier to adding more water to ice crystals and delaying ice recrystallization. Eniade et al. [182] demonstrated the IRI activity of carbon-linked antifreeze glycoprotein analogs. Due to the low degree of TH activity, these compounds may prove useful for cryopreservation. Inspired by hydration, more small molecules such as carbohydrate-based surfactants [183], facially amphiphatic glycopolymers [184] and metallohelices [185] are designed to inhibit ice recrystallization, revealing broad prospects for further development.

**Electrostatic interaction.** Polyampholytes [186], one kind of polymer that contains a mixture of cationic and anionic side chains, are also categorized as diffusion inhibition. Mitchell et al. [187] quantitatively analyzed the IRI ability of Poly(aminoethyl methacrylate) with different ratios of cationic and anionic on the side chains. As a result, the polyampholytes only exhibited strong IRI activity when the ratio of cationic to anionic was near 1:1, indicating that charge balance is essential. To investigate the inhibition mechanism, Matsumura et al. [188] used solid-state nuclear magnetic resonance spectroscopy to monitor the polymer-chain dynamic and the mobilities of water molecules in a carboxylated poly-L-lysine solution at low temperatures. The experiments revealed that the mobilities of water and polymer-chain were restricted increasingly with the decrease in temperature, indicating that the solution viscosity increased as well. It was ascribed to electrostatic interactions between the negatively and positively charged groups present in the polyampholytes, resulted in the aggregation of polymer molecules. The aggregated matrix contained water molecules and restricted the diffusion of water molecules between adjacent ice crystals. It is also an interpretation of why the best IRI activity can be achieved when the ratio of cationic and anionic groups is 1:1.

#### 4.3. Measurement of recrystallization rates

The ability to inhibit ice recrystallization is a very desirable property for cryopreservation. To determine the extent of IRI activity, a compound possesses, several assays have been developed to assess changes in ice crystal size, and the so-called “splat assay” and “sandwich assay” are the most commonly used in experiments [133,189].

In the case of splat assay [190], analytes are usually dissolved in 1~100 mM phosphate-buffered saline buffer. As shown in Fig. 14A, a 10 μL droplet of the solution is released 2 m above a polished aluminum plate pre-cooled to -78 °C by dry ice, generating a frozen wafer composed of very fine-grained ice. Then, using a pre-cooled spatula and tweezers carefully push the frozen wafer onto a glass coverslip and place it onto a cryostage. After a 30 min

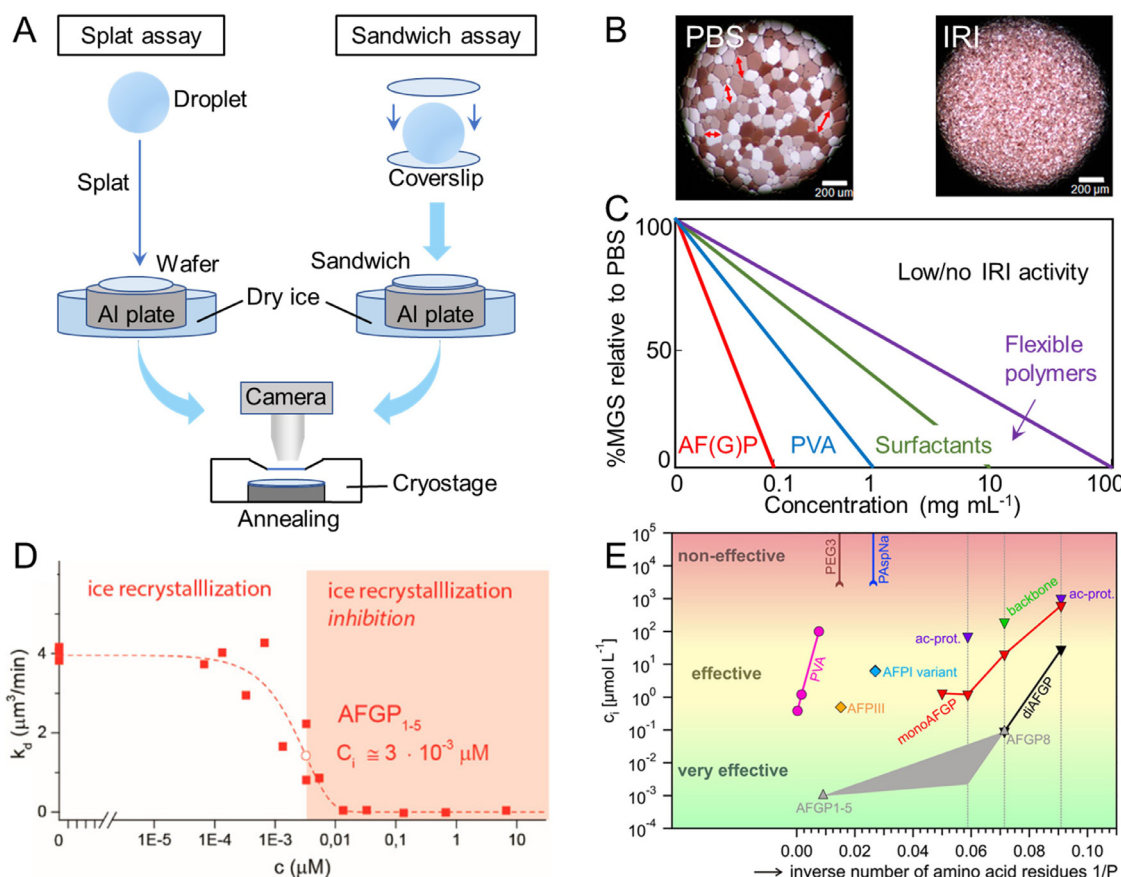


**Fig. 14.** IRI activity measurement. (A) Schematic of splat assay (left) and sandwich assay (right). (B) Example micrographs showing ice crystals grown in phosphate-buffered saline (PBS) buffer alone (left) and with IRI agents (right) [160]. (C) Summary of the range of activities observed for different classes of IRI agents [191]. (D) Corresponding ice recrystallization rate constant as a function of AFGP [193]. The AFGP shows IRI activity when the concentration is higher than  $c_i$ . (E) IRI concentration  $c_i$  as a function of the inverse number of amino acid residues  $1/P$  for several AFGPs and their analogs as well as for synthetic polymers [194]. For the polymers PVA, PEG3, and poly(aspartic acid) (PAspNa), which do not contain amino acids,  $P$  is the weight-average degree of polymerization. The gray area for the natural AFGP indicates the range of anticipated  $c_i$  at intermediate number of amino acid residues between AFGP1-5 and AFGP8, for which no data are available. The values for PEG3 and PAspNa correspond to the maximum concentration tested without signs of activity.

annealing time at  $-6\sim-8$  °C, the ice crystals recrystallize to larger mean grain size (MGS) and are photographed (Fig. 14B). The IRI activity is quantified based on measurements of the MGS after a certain time. Using this method, we can compare IRI activity between different types or concentrations of IRI agents. For example, Biggs et al. [191] provided a concise comparison of a range of natural and synthetic materials that are known to have IRI. They presented the MGS versus the agent concentration through the splat assay and divided them into four zones. The most active are AFPs and antifreeze glycoproteins (AFGPs), which function at sub 0.1 mg mL<sup>-1</sup>. The three other intervals are 0.1~1 mg mL<sup>-1</sup>, 1~10 mg mL<sup>-1</sup>, and 10~100 mg mL<sup>-1</sup>, respectively (Fig. 14C). Through this framework, we can analyze the IRI activity of new inhibitors more comprehensively.

Different from the splat assay, in the sandwich assay [192], analytes are dissolved in 18~45% sucrose solution. As shown in Fig. 14A, a 1 μL droplet of the solution is squashed between two coverslips to ensure even distribution. Then the coverslip sandwich is transferred to the pre-cooled aluminum plate with dry ice and maintained for 1 min. Subsequently, transfer the sandwich to a cryostage for 30~60 min to allow annealing at  $-6\sim-8$  °C. There is also an alternative approach for sandwich assay [132]. The coverslip sandwich can be directly transferred to the cryostage using liquid nitrogen cooling instead of placed into a pre-cooled environment with dry ice. Each sample is cooled from room temperature to -50 °C with a cooling rate of 20 °C min<sup>-1</sup> to induce multiple ice nucleation events. Then the polycrystalline ice sample is

reheated to the final annealing temperature at a warming rate of 10 °C min<sup>-1</sup>. After starting annealing, it is required to record the images by optical microscopy at a set time interval of  $t$ . The number and size of ice crystals are determined as a function of time and analyzed with LSW theory to extract the rate coefficient for ice recrystallization (Eq. (26)). When at low IRI agent concentrations, the ice recrystallization rate is diffusion-limited. But when IRI agent concentration is high enough, the ice recrystallization rate is limited by the ice-to-liquid and liquid-to-ice transfer, due to the adsorption of IRI agent to ice (Fig. 14D [193]). Thus, this method is usually used to determine the inhibitory concentration  $c_i$ . Budke et al. [194] also investigated the IRI efficacy of a large number of IRI agents, including natural AF(G)Ps, several synthetic AFGP analogs, as well as synthetic polymers. The lower the inhibitory concentration  $c_i$ , the more effective of IRI agent. After a comprehensive experiment, some AFGPs show very effective IRI activity ( $c_i < 10^{-1}$  μmol L<sup>-1</sup>). PVA, nature AFPs and their mimics are classified to effective compounds ( $10^{-1} < c_i < 10^3$  μmol L<sup>-1</sup>), while PEG3 and poly(aspartic acid) are classified to non-effective compounds ( $c_i > 10^3$  μmol L<sup>-1</sup>), as shown in Fig. 14E.

#### 4.4. Control strategies for recrystallization

AF(G)Ps and bioinspired materials have shown great potential in cryopreservation and the applications in cryopreservation of biomaterials are listed in Table 3. There are some key points worth noting for practice. Firstly, IRI agents have larger molecular weight

**Table 3**  
Control strategies for ice recrystallization.

Mechanisms	Control strategies	Materials	Biomaterials	Survival	Biocompatibility	Ref.
Adsorption inhibition	AF(G)Ps	AFP I	Escherichia coli	57.8%	✓	[197]
		AFP III	A549 cells	60%	✓	[195]
		AFGP <sub>1–5</sub>	Human RBCs	24%	✗	[196]
		AFGP <sub>1–5</sub> -ipp	Human RBCs	55%	✓	[196]
		GO	Horse sperm	71.3%	✓	[152]
	Nanomaterials	OQCN	sheep RBCs	~55%	✓	[153]
		GO-MoS <sub>2</sub>	HUVECs	>70%	✓	[130]
		Zr-MOF	Human RBCs	~40%	✓	[155]
		GO-Fe <sub>3</sub> O <sub>4</sub>	Stem cells	80.1%	✓	[198]
		G-CD	Sheep RBCs	~60%	✓	[199]
Diffusion inhibition	Polymers	WSe <sub>2</sub> -PVP	HUVECs	83.4%	✓	[200]
		PVA	Sheep RBCs	~80%	✓	[201]
		Polyproline	A549 cells	53%	✓	[202]
		L-proline	oocytes	99.11%	✓	[203]
		C-AFGP	WRL-68	~70%	✓	[204]
	Small molecules	Trehalose	WRL-68	~60%	✓	[106]
		COOH-PLL	L929 cells	~95%	✓	[205]
		DMAEMA-MAA	L929 cells	~90%	✓	[206]
		DMAPMA-AA	3T3 cells	~70%	✓	[207]

AFGP<sub>1–5</sub>-ipp: AFGP<sub>1–5</sub>-isopropylidene; GO-MoS<sub>2</sub>: graphene oxide and molybdenum disulfide ; Zr-MOF: zirconium-based metal-organic framework; G-CD: carbon dots from glucose; WSe<sub>2</sub>-PVP: tungsten diselenide-polyvinyl pyrrolidone; C-AFGP: carbon-linked AFGP; COOH-PLL: carboxylated poly-L-lysine; DMAEMA-MAA: 2-dimethylaminoethyl methacrylate-methacrylic acid; DMAPMA-AA: N-dimethylaminopropyl methacrylamide-acrylic acid.

than permeating CPAs and are difficult to penetrate in cells, thus usually acting in extracellular solution [195]. The addition of IRI agents results in the formation of tiny extracellular ice, which is less damaging to cells. Tomas et al. [195] explored the intracellular effect of AFP III. They delivered the AFP into A549 cells by using a cell-penetrating peptide and analyzed the recovery rate of cells. The presence of extracellular improved recovery rate to near 60% while intracellular AFP showed a recovery rate near 40%, attributed to the fact that intracellular AFP is toxic to cells and even leads to gene variation. Secondly, IRI activity is not the only standard for selection in cryopreservation and good biocompatibility is important as well. Sun et al. [196] investigated the cryopreservation efficiency of original AFGP<sub>1–5</sub> and chemically modified AFGP<sub>1–5</sub>-isopropylidene. Though the IRI activity of AFGP<sub>1–5</sub>-isopropylidene is weaker than AFGP<sub>1–5</sub>, it can enhance the interaction between AFGP and cell membranes, increasing the cell recovery of red blood cells from 24% to 55%. Therefore, membrane stabilization ability is another key factor for IRI agents in cryopreservation.

## 5. Summary and outlook

As highlighted in section 1, cryopreservation is imperative for the long-term storage of biomaterials, but the greatest limitation is the ice formation at low temperatures. This review systematically introduces the relationship between advanced strategies and ice control mechanisms based on the framework of ice formation: nucleation, growth, and recrystallization. Ice nucleation can be described by CNT and through the expression of nucleation rate, we analyze the key factors affecting nucleation: melting temperature, interfacial tension, shape factor, and kinetic prefactor. Subsequently, we present the theoretical model of ice growth in CPA solutions and find out that ice growth is mainly affected by solution viscosity and cooling/warming rate. Only if the cooling rate is higher than the CCR of CPA solutions can vitrification be achieved, and the warming rate needs to be higher than the CWR to avoid devitrification during warming. Ultimately, we discuss the phenomenon of ice recrystallization and the underlying mechanisms of IRI, including adsorption inhibition and diffusion inhibition. Furthermore, we introduce related research methods and control strategies corresponding to the three processes. Overall, ice

control is vital to achieving high-efficiency cryopreservation and each process of ice formation deserves in-depth study.

Though cryopreservation has made remarkable breakthroughs in recent years due to the rapid development of ice-control materials and biotechnologies, there are still some challenging points:

- Underlying mechanisms of CPA molecules regulating ice formation. Firstly, ice nucleation occurs at the nanoscale and is unable to be observed by experimental methods, resulting in still unclear molecular mechanisms of nucleation. And due to the stochastic nature of nucleation, the estimation of the nucleation rate has inevitable errors. Molecular dynamic simulations have been proven to be of utmost importance in unraveling the underlying mechanisms and can give us molecular insights into nucleation [87], including critical nucleus size, nucleation barrier, nucleation rate, etc. Unfortunately, molecular dynamic simulations for the nucleation rates of CPA solutions are rare, and one major limitation is that force fields remain imperfect and in short supply for many CPA molecules. Secondly, the ice growth model is still incomplete, and some factors affecting the model are not considered, such as the mutual influence of adjacent crystals, the irregular growth of ice, and non-diffusion control growth, etc. Thirdly, the IRI mechanisms of IRI agents are still unclear, depending on the interaction of IRI molecules with water/ice. Besides, the effect of 3-dimensional structures or key groups of IRI agents on ice control remains to be determined.
- Development of novel high-efficiency, biocompatible CPAs. Traditional CPAs like DMSO will cause inevitable toxicity to biomaterials, resulting in inefficient cryopreservation. Recently, many innovative materials (nanomaterials [208], synthetic polymers [141], hydrogels [209,210], etc.) have been utilized for ice control, which can be used to analyze the characteristic structures and protection mechanisms. It is inspiring for us to establish a programmed protocol to develop novel CPAs based on the mechanisms, which mainly focus on efficiency, biocompatibility, and practicality.
- Development of fast uniform cooling/warming methods. Vitrification can be facilitated by not only the addition of CPAs but also the application of fast cooling/warming. In this review, some advanced cooling/warming methods are introduced. However, rapid cooling methods are mainly applied to the vitrification of cells, difficult to generalize to tissues/organs. Notably,

vitrification under rapid cooling rates is accompanied by a Leidenfrost phenomenon, which impedes the heat transfer to cool the samples [211]. Therefore, the development of rapid uniform cooling/warming technologies and optimization of heat transfer will go a long way for cryopreservation.

4. Advanced engineering strategies for cryopreservation of biomaterials. To date, some engineering strategies such as trehalose delivery [212–214], cell encapsulation [215,216], and cell nanocoating [217] have been used to suppress ice and reduce cell injury in cryopreservation. These approaches are promising, but whether they have irreversible effects on cell viability remains to be investigated.

In conclusion, this review offers a systematic introduction on mechanisms and control strategies of ice nucleation, growth, and recrystallization. With the rapid development of biochemistry, bioengineering, and computer science, there are bound to be more insights into ice control and cryopreservation, alleviating the current situation of organ shortage. We anticipate this review will provide a general overview and serve as a stepping-stone for those interested in cryopreservation.

### Declaration of Competing Interest

The authors declared that they have no conflicts of interest to this work.

### Acknowledgments

This work was supported by the National Natural Science Foundation of China (Grant No. 52076115) and the Beijing Natural Science Foundation (Grant No. 3212019).

### References

- [1] J.K. Lewis, J.C. Bischof, I. Braslavsky, K.G. Brockbank, G.M. Fahy, B.J. Fuller, Y. Rabin, A. Tocchio, E.J. Woods, B.G. Wowk, J.P. Acker, S. Giwa, The grand challenges of organ banking: proceedings from the first global summit on complex tissue cryopreservation, *Cryobiology* 72 (2) (2016) 169–182, doi:10.1016/j.cryobiol.2015.12.001.
- [2] S. Giwa, J.K. Lewis, L. Alvarez, R. Langer, A.E. Roth, G.M. Church, J.F. Markmann, D.H. Sachs, A. Chandraker, J.A. Wertheim, M. Rothblatt, E.S. Boydlen, E. Eidbo, W.P.A. Lee, B. Pomahac, G. Brandacher, D.M. Weinstock, G. Elliott, D. Nelson, R.J. Acker, K. Uygun, B. Schmalz, B.P. Weegman, A. Tocchio, G.M. Fahy, K.B. Storey, B. Rubinsky, J. Bischof, J.A.W. Elliott, T.K. Woodruff, G.J. Morris, U. Demirci, K.G.M. Brockbank, E.J. Woods, R.N. Ben, J.G. Baust, D. Gao, B. Fuller, Y. Rabin, D.C. Kravitz, M.J. Taylor, M. Toner, The promise of organ and tissue preservation to transform medicine, *Nat. Biotechnol.* 35 (6) (2017) 530–542, doi:10.1038/nbt.3889.
- [3] E.J. Woods, S.F. Mullen, Organ preservation: cryobiology and beyond, *Curr. Stem Cell Rep.* 2 (2) (2016) 104–117, doi:10.1007/s40778-016-0042-8.
- [4] M.J. Taylor, B.P. Weegman, S.C. Baicu, S.E. Giwa, New approaches to cryopreservation of cells, tissues, and organs, *Transfus. Med. Hemother.* 46 (3) (2019) 197–215, doi:10.1159/000499453.
- [5] E.B. Finger, J.C. Bischof, Cryopreservation by vitrification: a promising approach for transplant organ banking, *Curr. Opin. Organ Transplant.* 23 (3) (2018) 353–360, doi:10.1097/MOT.0000000000000534.
- [6] S. Bojic, A. Murray, B.L. Bentley, R. Spindler, P. Pawlik, J.L. Cordeiro, R. Bauer, J.P. de Magalhaes, Winter is coming: the future of cryopreservation, *BMC Biol.* 19 (1) (2021) 1–20, doi:10.1186/s12915-021-00976-8.
- [7] M. Dou, C. Lu, W. Rao, Bioinspired materials and technology for advanced cryopreservation, *Trends Biotechnol.* 40 (1) (2022) 93–106, doi:10.1016/j.tibtech.2021.06.004.
- [8] J. Yang, C. Pan, X. Sui, N. Cai, J. Zhang, Y. Zhu, L. Zhang, The hypothermic preservation of mammalian cells with assembling extracellular-matrix-mimetic microparticles, *J. Mater. Chem. B* 5 (8) (2017) 1535–1541, doi:10.1039/c6tb03206k.
- [9] L. Jing, L. Yao, M. Zhao, L.P. Peng, M. Liu, Organ preservation: from the past to the future, *Acta Pharmacol. Sin.* 39 (5) (2018) 845–857, doi:10.1038/aps.2017.182.
- [10] Y. Ma, L. Gao, Y. Tian, P. Chen, J. Yang, L. Zhang, Advanced biomaterials in cell preservation: hypothermic preservation and cryopreservation, *Acta Biomater.* 131 (2021) 97–116, doi:10.1016/j.actbio.2021.07.001.
- [11] A. Sharma, J.S. Rao, Z. Han, L. Gangwar, B. Namsrai, Z. Gao, H.L. Ring, E. Magnuson, M. Etheridge, B. Wowk, G.M. Fahy, M. Garwood, E.B. Finger, J.C. Bischof, Vitrification and nanowarming of kidneys, *Adv. Sci.* (2021) e2101691, doi:10.1002/advs.202101691.
- [12] T.A. Berendsen, B.G. Bruinsma, C.F. Puts, N. Saeidi, O.B. Usta, B.E. Uygun, M.L. Izamis, M. Toner, M.L. Yarmush, K. Uygun, Supercooling enables long-term transplantation survival following 4 days of liver preservation, *Nat. Med.* 20 (7) (2014) 790–793, doi:10.1038/nm.3588.
- [13] B.G. Bruinsma, T.A. Berendsen, M.L. Izamis, H. Yeh, M.L. Yarmush, K. Uygun, Supercooling preservation and transplantation of the rat liver, *Nat. Protoc.* 10 (3) (2015) 484–494, doi:10.1038/nprot.2015.011.
- [14] H. Huang, M.L. Yarmush, O.B. Usta, Long-term deep-supercooling of large-volume water and red cell suspensions via surface sealing with immiscible liquids, *Nat. Commun.* 9 (1) (2018) 3201, doi:10.1038/s41467-018-05636-0.
- [15] P. Mazur, Cryobiology: the freezing of biological systems, *Science* 168 (3934) (1970) 939–949, doi:10.1126/science.168.3934.939.
- [16] P.L. Steponkus, S.P. Myers, D.V. Lynch, L. Gardner, V. Bronshteyn, S.P. Leibo, W.F. Rall, R.E. Pitt, T.T. Lin, R.J. MacIntyre, Cryopreservation of drosophila melanogaster embryos, *Nature* 345 (6271) (1990) 170–172, doi:10.1038/345170a0.
- [17] J.O. Karlsson, Cryopreservation: freezing and vitrification, *Science* 296 (5568) (2002) 655–656, doi:10.1126/science.296.5568.655d.
- [18] K.A. Murray, M.I. Gibson, Chemical approaches to cryopreservation, *Nat. Rev. Chem.* 6 (8) (2022) 579–593, doi:10.1038/s41570-022-00407-4.
- [19] E.J. Woods, S. Thirumala, S.S. Badhe-Buchanan, D. Clarke, A.J. Mathew, Off the shelf cellular therapeutics: factors to consider during cryopreservation and storage of human cells for clinical use, *Cytotherapy* 18 (6) (2016) 697–711, doi:10.1016/j.jcyt.2016.03.295.
- [20] T. Chang, G. Zhao, Ice inhibition for cryopreservation: materials, strategies, and challenges, *Adv. Sci.* 8 (6) (2021) 2002425, doi:10.1002/advs.202002425.
- [21] G.D. Elliott, S. Wang, B.J. Fuller, Cryoprotectants: a review of the actions and applications of cryoprotective solutes that modulate cell recovery from ultralow temperatures, *Cryobiology* 76 (2017) 74–91, doi:10.1016/j.cryobiol.2017.04.004.
- [22] H. Huang, X. He, M.L. Yarmush, Advanced technologies for the preservation of mammalian biospecimens, *Nat. Biomed. Eng.* 5 (8) (2021) 793–804, doi:10.1038/s41551-021-00784-z.
- [23] P. Mazur, S.P. Leibo, E.H. Chu, A two-factor hypothesis of freezing injury: evidence from Chinese hamster tissue-culture cells, *Exp. Cell Res.* 71 (2) (1972) 345–355, doi:10.1016/0014-4827(72)90303-5.
- [24] P. Mazur, The role of cell membranes in the freezing of yeast and other single cells, *Ann. N. Y. Acad. Sci.* 125 (2) (1965) 658–676, doi:10.1111/j.1749-6632.1965.tb45420.x.
- [25] M. Toner, E.G. Cravalho, M. Karel, Thermodynamics and kinetics of intracellular ice formation during freezing of biological cells, *J. Appl. Phys.* 67 (3) (1990) 1582–1593, doi:10.1063/1.345670.
- [26] P.L. Steponkus, D.G. Stout, J. Wolfe, R.V.E. Lovelace, Possible role of transient electric fields in freezing-induced membrane destabilization, *J. Membr. Biol.* 85 (3) (1985) 191–198, doi:10.1007/bf01871513.
- [27] K. Muldrew, L.E. McGann, Mechanisms of intracellular ice formation, *Biophys. J.* 57 (3) (1990) 525–532, doi:10.1016/s0006-3495(90)82568-6.
- [28] Z. Gao, B. Namsrai, Z. Han, P. Joshi, J.S. Rao, V. Ravikumar, A. Sharma, H.L. Ring, D. Idiyatullin, E.C. Magnuson, P.A. Iaizzo, E.G. Tolkacheva, M. Garwood, Y. Rabin, M. Etheridge, E.B. Finger, J.C. Bischof, Vitrification and rewarming of magnetic nanoparticle loaded rat hearts, *Adv. Mater. Technol.* 7 (3) (2021) 2100873, doi:10.1002/admt.202100873.
- [29] L. Zhan, M.G. Li, T. Hays, J. Bischof, Cryopreservation method for drosophila melanogaster embryos, *Nat. Commun.* 12 (1) (2021) 2412, doi:10.1038/s41467-021-22694-z.
- [30] M. Lin, H. Cao, Q. Meng, J. Li, P. Jiang, Insights into the crystallization and vitrification of cryopreserved cells, *Cryobiology* 106 (2022) 13–23, doi:10.1016/j.cryobiol.2022.04.008.
- [31] L. Zhan, J.S. Rao, N. Sethia, M.Q. Slama, Z. Han, D. Tobolt, M. Etheridge, Q.P. Peterson, C.S. Dutcher, J.C. Bischof, E.B. Finger, Pancreatic islet cryopreservation by vitrification achieves high viability, function, recovery and clinical scalability for transplantation, *Nat. Med.* 28 (4) (2022) 798–808, doi:10.1038/s41591-022-01718-1.
- [32] J.B. Hopkins, R. Badeau, M. Warkentin, R.E. Thorne, Effect of common cryoprotectants on critical warming rates and ice formation in aqueous solutions, *Cryobiology* 65 (3) (2012) 169–178, doi:10.1016/j.cryobiol.2012.05.010.
- [33] C. Polge, A.U. Smith, A.S. Parkes, Revival of spermatozoa after vitrification and dehydration at low temperatures, *Nature* 164 (4172) (1949) 666, doi:10.1038/164666a0.
- [34] J.E. Lovelock, M.W. Bishop, Prevention of freezing damage to living cells by dimethyl sulphoxide, *Nature* 183 (4672) (1959) 1394–1395, doi:10.1038/1831394a0.
- [35] B.P. Best, Cryoprotectant toxicity: facts, issues, and questions, *Rejuvenation Res.* 18 (5) (2015) 422–436, doi:10.1089/rej.2014.1656.
- [36] Z. Liu, X. Zheng, J. Wang, Bioinspired ice-binding materials for tissue and organ cryopreservation, *J. Am. Chem. Soc.* 144 (13) (2022) 5685–5701, doi:10.1021/jacs.2c00203.
- [37] Z. Wang, C. Valenzuela, J. Wu, Y. Chen, L. Wang, W. Feng, Bioinspired freeze-tolerant soft materials: design, properties, and applications, *Small* (2022) e2201597, doi:10.1002/smll.202201597.
- [38] J.C. Bischof, K.R. Diller, From nanowarming to thermoregulation: new multi-scale applications of bioheat transfer, *Annu. Rev. Biomed. Eng.* 20 (2018) 301–327, doi:10.1146/annurev-bioeng-071516-044532.
- [39] R. Raju, S.J. Bryant, B.L. Wilkinson, G. Bryant, The need for novel cryoprotectants and cryopreservation protocols: insights into the importance of bio-

- physical investigation and cell permeability, *Biochim. Biophys. Acta, Gen. Subj.* 1865 (1) (2021) 129749, doi:10.1016/j.bbagen.2020.129749.
- [40] M. Bar Dolev, I. Braslavsky, P.L. Davies, Ice-binding proteins and their function, *Annu. Rev. Biochem.* 85 (2016) 515–542, doi:10.1146/annurev-biochem-060815-014546.
- [41] X. Wu, F. Yao, H. Zhang, J. Li, Antifreeze proteins and their biomimetics for cell cryopreservation: mechanism, function and application-a review, *Int. J. Biol. Macromol.* 192 (2021) 1276–1291, doi:10.1016/j.ijbiomac.2021.09.211.
- [42] A. Baskaran, M. Kaari, G. Venugopal, R. Manikkam, J. Joseph, P.V. Bhaskar, Anti freeze proteins (AFP): properties, sources and applications - a review, *Int. J. Biol. Macromol.* 189 (2021) 292–305, doi:10.1016/j.ijbiomac.2021.08.105.
- [43] Z. He, K. Liu, J. Wang, Bioinspired materials for controlling ice nucleation, growth, and recrystallization, *Acc. Chem. Res.* 51 (5) (2018) 1082–1091, doi:10.1021/acs.accounts.7b00528.
- [44] M. Dalvi-Isfahan, N. Hamdam, E. Xanthakis, A. Le-Bail, Review on the control of ice nucleation by ultrasounds waves, electric and magnetic fields, *J. Food Eng.* 195 (2017) 222–234, doi:10.1016/j.jfoodeng.2016.10.001.
- [45] Z. Zhu, Q. Zhou, D.-W. Sun, Measuring and controlling ice crystallization in frozen foods: a review of recent developments, *Trends Food Sci. Technol.* 90 (2019) 13–25, doi:10.1016/j.tifs.2019.05.012.
- [46] Z. Zhang, X.Y. Liu, Control of ice nucleation: freezing and antifreeze strategies, *Chem. Soc. Rev.* 47 (18) (2018) 7116–7139, doi:10.1039/c8cs00626a.
- [47] I.V. Markov, *Crystal Growth for Beginners: Fundamentals of Nucleation, Crystal Growth and Epitaxy*, 3rd, World Scientific, 2016.
- [48] A.K. Balcerzak, C.J. Capicciotti, J.G. Briard, R.N. Ben, Designing ice recrystallization inhibitors: from antifreeze (glyco)proteins to small molecules, *RSC Adv.* 4 (80) (2014) 42682–42696, doi:10.1039/c4ra06893a.
- [49] J.W. Gibbs, *The collected works of J. Willard Gibbs*, Longmans, Green and Co.: New York, 1928.
- [50] M. Volmer, A. Weber, Germ-formation in oversaturated figures, *Z. Phys. Chem.* 119 (3/4) (1926) 277–301.
- [51] R. Becker, W. Döring, Kinetische behandlung der keimbildung in übersättigten dämpfen, *Ann. Phys.* 416 (8) (1935) 719–752, doi:10.1002/andp.19354160806.
- [52] J. Frenkel, A general theory of heterophase fluctuations and pretransition phenomena, *J. Chem. Phys.* 7 (7) (1939) 538–547, doi:10.1063/1.1750484.
- [53] L. Ickes, A. Welti, C. Hoose, U. Lohmann, Classical nucleation theory of homogeneous freezing of water: thermodynamic and kinetic parameters, *Phys. Chem. Chem. Phys.* 17 (8) (2015) 5514–5537, doi:10.1039/c4cp04184d.
- [54] Q. Li, Z. Guo, Fundamentals of icing and common strategies for designing biomimetic anti-icing surfaces, *J. Mater. Chem. A* 6 (28) (2018) 13549–13581, doi:10.1039/c8ta03259a.
- [55] M. Awan, I. Buriak, R. Fleck, B. Fuller, A. Goltsev, J. Kerby, M. Lowdell, P. Mericka, A. Petrenko, Y. Petrenko, O. Rogulska, A. Stolzing, G.N. Stacey, Dimethyl sulfoxide: a central player since the dawn of cryobiology, is efficacy balanced by toxicity? *Regen. Med.* 15 (3) (2020) 1463–1491, doi:10.2217/rme-2019-0145.
- [56] I.A. Borin, M.S. Skaf, Molecular association between water and dimethyl sulfoxide in solution: a molecular dynamics simulation study, *J. Chem. Phys.* 110 (13) (1999) 6412–6420, doi:10.1063/1.478544.
- [57] A. Vishnyakov, A.P. Lyubartsev, A. Laaksonen, Molecular dynamics simulations of dimethyl sulfoxide and dimethyl sulfoxide-water mixture, *J. Phys. Chem. A* 105 (10) (2001) 1702–1710, doi:10.1021/jp0007336.
- [58] N. Zhang, W. Li, C. Chen, J. Zuo, Molecular dynamics simulation of aggregation in dimethyl sulfoxide water binary mixture, *Comput. Theor. Chem.* 1017 (2013) 126–135, doi:10.1016/j.comptc.2013.05.018.
- [59] D.H. Rasmussen, A.P. MacKenzie, Phase diagram for the system water-dimethylsulphoxide, *Nature* 220 (5174) (1968) 1315–1317, doi:10.1038/2201315a0.
- [60] J.O. Karlsson, Effects of solution composition on the theoretical prediction of ice nucleation kinetics and thermodynamics, *Cryobiology* 60 (1) (2010) 43–51, doi:10.1016/j.cryobiol.2009.07.004.
- [61] L. Weng, S.L. Stott, M. Toner, Exploring dynamics and structure of biomolecules, cryoprotectants, and water using molecular dynamics simulations: implications for biostabilization and biopreservation, *Annu. Rev. Biomed. Eng.* 21 (2019) 1–31, doi:10.1146/annurev-bioeng-060418-052130.
- [62] H. Kanno, R.J. Speedy, C.A. Angell, Supercooling of water to -92 °C under pressure, *Science* 189 (4206) (1975) 880–881, doi:10.1126/science.189.4206.880.
- [63] T. Loerting, K. Winkel, M. Seidl, M. Bauer, C. Mitterdorfer, P.H. Handle, C.G. Salzmann, E. Mayer, J.L. Finney, D.T. Bowron, How many amorphous ices are there? *Phys. Chem. Chem. Phys.* 13 (19) (2011) 8783–8794, doi:10.1039/c0cp02600j.
- [64] J.R. Espinosa, G.D. Soria, J. Ramirez, C. Valeriani, C. Vega, E. Sanz, Role of salt, pressure, and water activity on homogeneous ice nucleation, *J. Phys. Chem. Lett.* 8 (18) (2017) 4486–4491, doi:10.1021/acs.jpclett.7b01551.
- [65] P.W. Wilson, K.E. Osterday, A.F. Heneghan, A.D. Haymet, Type I antifreeze proteins enhance ice nucleation above certain concentrations, *J. Biol. Chem.* 285 (45) (2010) 34741–34745, doi:10.1074/jbc.M110.171983.
- [66] L. Eickhoff, K. Dreischmeier, A. Zipori, V. Sirotinskaya, C. Adar, N. Reicher, I. Braslavsky, Y. Rudich, T. Koop, Contrasting behavior of antifreeze proteins: ice growth inhibitors and ice nucleation promoters, *J. Phys. Chem. Lett.* 10 (5) (2019) 966–972, doi:10.1021/acs.jpclett.8b03719.
- [67] N. Du, X.Y. Liu, C.L. Hew, Ice nucleation inhibition: mechanism of antifreeze by antifreeze protein, *J. Biol. Chem.* 278 (38) (2003) 36000–36004, doi:10.1074/jbc.M305222200.
- [68] T. Inada, T. Koyama, F. Goto, T. Seto, Ice nucleation in emulsified aqueous solutions of antifreeze protein type III and poly(vinyl alcohol), *J. Phys. Chem. B* 115 (24) (2011) 7914–7922, doi:10.1021/jp111745v.
- [69] K. Liu, C. Wang, J. Ma, G. Shi, X. Yao, H. Fang, Y. Song, J. Wang, Janus effect of antifreeze proteins on ice nucleation, *Proc. Natl. Acad. Sci. U.S.A.* 113 (51) (2016) 14739–14744, doi:10.1073/pnas.1614379114.
- [70] M. Orlowska, M. Havet, A. Le-Bail, Controlled ice nucleation under high voltage dc electrostatic field conditions, *Food Res. Int.* 42 (7) (2009) 879–884, doi:10.1016/j.foodres.2009.03.015.
- [71] J.Y. Yan, G.N. Patey, Heterogeneous ice nucleation induced by electric fields, *J. Phys. Chem. Lett.* 2 (20) (2011) 2555–2559, doi:10.1021/jz201113m.
- [72] L. Otero, A.C. Rodriguez, M. Perez-Mateos, P.D. Sanz, Effects of magnetic fields on freezing: application to biological products, *Compr. Rev. Food Sci. Food Saf.* 15 (3) (2016) 646–667, doi:10.1111/1541-4337.12202.
- [73] X.Y. Liu, A new kinetic model for three-dimensional heterogeneous nucleation, *J. Chem. Phys.* 111 (4) (1999) 1628–1635, doi:10.1063/1.479391.
- [74] S.J. Cooper, C.E. Nicholson, J. Liu, A simple classical model for predicting onset crystallization temperatures on curved substrates and its implications for phase transitions in confined volumes, *J. Chem. Phys.* 129 (12) (2008) 124715, doi:10.1063/1.2977993.
- [75] X.Y. Liu, N. Du, Zero-sized effect of nano-particles and inverse homogeneous nucleation. Principles of freezing and antifreeze, *J. Biol. Chem.* 279 (7) (2004) 6124–6131, doi:10.1074/jbc.M310487200.
- [76] G. Bai, D. Gao, Z. Liu, X. Zhou, J. Wang, Probing the critical nucleus size for ice formation with graphene oxide nanosheets, *Nature* 576 (7787) (2019) 437–441, doi:10.1038/s41586-019-1827-6.
- [77] R. Pandey, K. Usui, R.A. Livingstone, S.A. Fischer, J. Pfaendtner, E.H. Backus, Y. Nagata, J. Frohlich-Nowoisky, L. Schmuser, S. Mauri, J.F. Scheel, D.A. Knopf, U. Poschl, M. Bonn, T. Weidner, Ice-nucleating bacteria control the order and dynamics of interfacial water, *Sci. Adv.* 2 (4) (2016) e1501630, doi:10.1126/sciadv.1501630.
- [78] S.J. Roeters, T.W. Golbek, M. Bregnhøj, T. Drace, S. Alamdar, W. Roseboom, G. Kramer, T. Santl-Temkiv, K. Finster, J. Pfaendtner, S. Woutersen, T. Boesen, T. Weidner, Ice-nucleating proteins are activated by low temperatures to control the structure of interfacial water, *Nat. Commun.* 12 (1) (2021) 1183, doi:10.1038/s41467-021-21349-3.
- [79] Y. Qiu, A. Hudait, V. Molinero, How size and aggregation of ice-binding proteins control their ice nucleation efficiency, *J. Am. Chem. Soc.* 141 (18) (2019) 7439–7452, doi:10.1021/jacs.9b01854.
- [80] S.E. Lindow, D.C. Arny, C.D. Upper, Bacterial ice nucleation: a factor in frost injury to plants, *Plant Physiol.* 70 (4) (1982) 1084–1089, doi:10.1104/pp.70.4.1084.
- [81] G.R. Wood, A.G. Walton, Homogeneous nucleation kinetics of ice from water, *J. Appl. Phys.* 41 (7) (1970) 3027–3036, doi:10.1063/1.1659359.
- [82] S.I. Girshick, C. Chiu, Kinetic nucleation theory: a new expression for the rate of homogeneous nucleation from an ideal supersaturated vapor, *J. Chem. Phys.* 93 (2) (1990) 1273–1277, doi:10.1063/1.459191.
- [83] S. Auer, D. Frenkel, Prediction of absolute crystal-nucleation rate in hard-sphere colloids, *Nature* 409 (6823) (2001) 1020–1023, doi:10.1038/35059035.
- [84] X.Y. Liu, Interfacial effect of molecules on nucleation kinetics, *J. Phys. Chem. B* 105 (47) (2001) 11550–11558, doi:10.1021/jp010671z.
- [85] D.T. Wu, L. Gránásy, F. Spaepen, Nucleation and the solid liquid interfacial free energy, *MRS Bull.* 29 (12) (2004) 945–950, doi:10.1557/mrs2004.265.
- [86] J.W.P. Schmelzer, On the determination of the kinetic pre-factor in classical nucleation theory, *J. Non-Cryst. Solids* 356 (52–54) (2010) 2901–2907, doi:10.1016/j.jnoncrysol.2010.02.026.
- [87] G.C. Sosso, J. Chen, S.J. Cox, M. Fitzner, P. Pedevilla, A. Zen, A. Michaelides, Crystal nucleation in liquids: open questions and future challenges in molecular dynamics simulations, *Chem. Rev.* 116 (12) (2016) 7078–7116, doi:10.1021/acs.chemrev.5b00744.
- [88] V.I. Kalikmanov, *Nucleation Theory, Lecture Notes in Physics, volume 860, Springer, Heidelberg*, 2013.
- [89] G. Yu, R. Li, A. Hubel, Interfacial interactions of sucrose during cryopreservation detected by raman spectroscopy, *Langmuir* 35 (23) (2019) 7388–7395, doi:10.1021/acs.langmuir.8b01616.
- [90] L. Weng, G.D. Elliott, Dynamic and thermodynamic characteristics associated with the glass transition of amorphous trehalose-water mixtures, *Phys. Chem. Chem. Phys.* 16 (23) (2014) 11555–11565, doi:10.1039/c3cp55418j.
- [91] T. Congdon, B.T. Dean, J. Kasperek-Wright, C.I. Biggs, R. Notman, M.I. Gibson, Probing the biomimetic ice nucleation inhibition activity of poly(vinyl alcohol) and comparison to synthetic and biological polymers, *Biomacromolecules* 16 (9) (2015) 2820–2826, doi:10.1021/acs.biomac.5b00774.
- [92] C.I. Biggs, C. Packer, S. Hindmarsh, M. Walker, N.R. Wilson, J.P. Rourke, M.I. Gibson, Impact of sequential surface-modification of graphene oxide on ice nucleation, *Phys. Chem. Chem. Phys.* 19 (33) (2017) 21929–21932, doi:10.1039/c7cp03219f.
- [93] K. Li, S. Xu, W. Shi, M. He, H. Li, S. Li, X. Zhou, J. Wang, Y. Song, Investigating the effects of solid surfaces on ice nucleation, *Langmuir* 28 (29) (2012) 10749–10754, doi:10.1021/la3014915.
- [94] H. Laksmono, T.A. McQueen, J.A. Sellberg, N.D. Loh, C. Huang, D. Schlesinger, R.G. Sierra, C.Y. Hampton, D. Nordlund, M. Beye, A.V. Martin, A. Barty, M.M. Seibert, M. Messerschmidt, G.J. Williams, S. Boutet, K. Amann-Winkel, T. Loerting, L.G. Pettersson, M.J. Bogan, A. Nilsson, Anomalous behavior of the homogeneous ice nucleation rate in "no-man's land", *J. Phys. Chem. Lett.* 6 (14) (2015) 2826–2832, doi:10.1021/acs.jpclett.5b01164.

- [95] J.A. Sellberg, C. Huang, T.A. McQueen, N.D. Loh, H. Laksmono, D. Schlesinger, R.G. Sierra, D. Nordlund, C.Y. Hampton, D. Starodub, D.P. DePonte, M. Beye, C. Chen, A.V. Martin, A. Barty, K.T. Wikfeldt, T.M. Weiss, C. Caronna, J. Feldkamp, L.B. Skinner, M.M. Seibert, M. Messerschmidt, G.J. Williams, S. Boutet, L.G. Pettersson, M.J. Bogan, A. Nilsson, Ultrafast x-ray probing of water structure below the homogeneous ice nucleation temperature, *Nature* 510 (7505) (2014) 381–384, doi:10.1038/nature13266.
- [96] A. Manka, H. Pathak, S. Tanimura, J. Wolk, R. Strey, B.E. Wyslouzil, Freezing water in no-man's land, *Phys. Chem. Chem. Phys.* 14 (13) (2012) 4505–4516, doi:10.1039/c2cp23116f.
- [97] V. Buch, J.P. Devlin, *Water in Confining Geometries*, Springer Science & Business Media, 2003.
- [98] Y.S. Djikavaev, A. Tabazadeh, P. Hamill, H. Reiss, Thermodynamic conditions for the surface-stimulated crystallization of atmospheric droplets, *J. Phys. Chem. A* 106 (43) (2002) 10247–10253, doi:10.1021/jp021044s.
- [99] T. Kuhn, M.E. Earle, A.F. Khalizov, J.J. Sloan, Size dependence of volume and surface nucleation rates for homogeneous freezing of supercooled water droplets, *Atmos. Chem. Phys.* 11 (6) (2011) 2853–2861, doi:10.5194/acp-11-2853-2011.
- [100] G.J. Morris, E. Acton, Controlled ice nucleation in cryopreservation—a review, *Cryobiology* 66 (2) (2013) 85–92, doi:10.1016/j.cryobiol.2012.11.007.
- [101] J.D. Benson, A.J. Kearsey, A.Z. Higgins, Mathematical optimization of procedures for cryoprotectant equilibration using a toxicity cost function, *Cryobiology* 64 (3) (2012) 144–151, doi:10.1016/j.cryobiol.2012.01.001.
- [102] S. Kojima, M. Kaku, T. Kawata, H. Sumi, H. Shikata, T.R. Abonti, S. Kojima, T. Fujita, M. Motokawa, K. Tanne, Cryopreservation of rat mscs by use of a programmed freezer with magnetic field, *Cryobiology* 67 (3) (2013) 258–263, doi:10.1016/j.cryobiol.2013.08.003.
- [103] N. Greer, Freezing under pressure: a new method for cryopreservation, *Cryobiology* 70 (1) (2015) 66–70, doi:10.1016/j.cryobiol.2014.12.005.
- [104] Y.H. Ma, G.F. Qian, J. Li, G.R. Ding, S.L. Xu, Y. Zhou, G.Z. Guo, AC electric field enhances cryopreservation efficiency of sprague-dawley rat liver during a slow freezing procedure, *Biopreserv. Biobank.* 14 (1) (2016) 23–28, doi:10.1089/bio.2015.0042.
- [105] G. Missous, B. Thammavongs, V. Dieuleveaux, M. Gueguen, J.M. Panoff, Improvement of the cryopreservation of the fungal starter *Geotrichum candidum* by artificial nucleation and temperature downshift control, *Cryobiology* 55 (1) (2007) 66–71, doi:10.1016/j.cryobiol.2007.05.004.
- [106] J.L. Chaytor, J.M. Tokarek, L.K. Wu, M. Leclere, R.Y. Tam, C.J. Capicciotti, L. Guolla, E. von Moos, C.S. Findlay, D.S. Allan, R.N. Ben, Inhibiting ice recrystallization and optimization of cell viability after cryopreservation, *Glycobiology* 22 (1) (2012) 123–133, doi:10.1093/glycob/cwr115.
- [107] J.O. Karlsson, E.G. Cravalho, I.H. Borel Rinkes, R.G. Tompkins, M.L. Yarmush, M. Toner, Nucleation and growth of ice crystals inside cultured hepatocytes during freezing in the presence of dimethyl sulfoxide, *Biophys. J.* 65 (6) (1993) 2524–2536, doi:10.1016/s0006-3495(93)81319-5.
- [108] J.O.M. Karlsson, E.G. Cravalho, M. Toner, A model of diffusion limited ice growth inside biological cells during freezing, *J. Appl. Phys.* 75 (9) (1994) 4442–4455, doi:10.1063/1.355959.
- [109] G. Yang, A. Zhang, L.X. Xu, X. He, Modeling the cell-type dependence of diffusion-limited intracellular ice nucleation and growth during both vitrification and slow freezing, *J. Appl. Phys.* 105 (11) (2009) 114701.
- [110] G. Zhao, H. Takamatsu, X. He, The effect of solution nonideality on modeling transmembrane water transport and diffusion-limited intracellular ice formation during cryopreservation, *J. Appl. Phys.* 115 (14) (2014) 144701, doi:10.1063/1.4870826.
- [111] D.R. MacFarlane, M. Fragoulis, Theory of devitrification in multicomponent glass forming systems under diffusion control, *Phys. Chem. Glasses* 27 (6) (1986) 228–234.
- [112] P. Bruna, D. Crespo, R. González-Cinca, E. Pineda, On the validity of avrami formalism in primary crystallization, *J. Appl. Phys.* 100 (5) (2006) 054907, doi:10.1063/1.2337407.
- [113] X. Xue, H.-L. Jin, Z.-Z. He, J. Liu, Quantifying the growth rate and morphology of ice crystals growth in cryoprotectants via high-speed camera and cromicroscope, *J. Heat Transfer* 137 (9) (2015) 091020, doi:10.1115/1.4030236.
- [114] P. Mazur, S. Seki, I.L. Pinn, F.W. Kleinhans, K. Edashige, Extra- and intracellular ice formation in mouse oocytes, *Cryobiology* 51 (1) (2005) 29–53, doi:10.1016/j.cryobiol.2005.04.008.
- [115] S.L. Stott, J.O.M. Karlsson, Visualization of intracellular ice formation using high-speed video cromicroscopy, *Cryobiology* 58 (1) (2009) 84–95, doi:10.1016/j.cryobiol.2008.11.003.
- [116] T. Ninagawa, A. Eguchi, Y. Kawamura, T. Konishi, A. Narumi, A study on ice crystal formation behavior at intracellular freezing of plant cells using a high-speed camera, *Cryobiology* 73 (1) (2016) 20–29, doi:10.1016/j.cryobiol.2016.06.003.
- [117] Y. Wang, K. Zhu, X. Zhang, H. Ji, Applications of gray-level variation detection method to intracellular ice formation, *Cryobiology* 81 (2018) 81–87, doi:10.1016/j.cryobiol.2018.02.006.
- [118] P.M. Mehl, Nucleation and crystal growth in a vitrification solution tested for organ cryopreservation by vitrification, *Cryobiology* 30 (5) (1993) 509–518, doi:10.1006/cryo.1993.1051.
- [119] E. Bogdanova, A.M. Fureby, V. Kocherbitov, Influence of cooling rate on ice crystallization and melting in sucrose-water system, *J. Pharm. Sci.* (2022) 2030–2037, doi:10.1016/j.xphs.2022.01.027.
- [120] R.L. Sutton, Critical cooling rates to avoid ice crystallization in solutions of cryoprotective agents, *J. Chem. Soc., Faraday Trans.* 87 (1) (1991) 101–105, doi:10.1039/ft9918700101.
- [121] D.R. Uhlmann, A kinetic treatment of glass formation, *J. Non-Cryst. Solids* 7 (4) (1972) 337–348, doi:10.1016/0022-3093(72)90269-4.
- [122] D.R. MacFarlane, Continuous cooling (CT) diagrams and critical cooling rates: a direct method of calculation using the concept of additivity, *J. Non-Cryst. Solids* 53 (1–2) (1982) 61–72, doi:10.1016/0022-3093(82)90018-7.
- [123] M. Dou, C. Lu, J. Liu, W. Rao, Liquid helium enhanced vitrification efficiency of human bone-derived mesenchymal stem cells and human embryonic stem cells, *Bioengineering* 8 (11) (2021) 162, doi:10.3390/bioengineering8110162.
- [124] M. Shi, K. Ling, K.W. Yong, Y. Li, S. Feng, X. Zhang, B. Pingguan-Murphy, T.J. Lu, F. Xu, High-throughput non-contact vitrification of cell-laden droplets based on cell printing, *Sci. Rep.* 5 (2015) 17928, doi:10.1038/srep17928.
- [125] Y. Akiyama, M. Shinose, H. Watanabe, S. Yamada, Y. Kanda, Cryoprotectant-free cryopreservation of mammalian cells by superflash freezing, *Proc. Natl. Acad. Sci. U.S.A.* 116 (16) (2019) 7738–7743, doi:10.1073/pnas.1808645116.
- [126] N. Manuchehrabadi, Z. Gao, J. Zhang, H.L. Ring, Q. Shao, F. Liu, M. McDermott, A. Fok, Y. Rabin, K.G. Brockbank, M. Garwood, C.L. Haynes, J.C. Bischof, Improved tissue cryopreservation using inductive heating of magnetic nanoparticles, *Sci. Transl. Med.* 9 (379) (2017) eaah4586, doi:10.1126/scitranslmed.aah4586.
- [127] K. Khosla, Y. Wang, M. Hagedorn, Z. Qin, J. Bischof, Gold nanorod induced warming of embryos from the cryogenic state enhances viability, *ACS Nano* 11 (8) (2017) 7869–7878, doi:10.1021/acsnano.7b02216.
- [128] L. Zhan, Z. Han, Q. Shao, M.L. Etheridge, T. Hays, J.C. Bischof, Rapid joule heating improves vitrification based cryopreservation, *Nat. Commun.* 13 (1) (2022) 6017, doi:10.1038/s41467-022-33546-9.
- [129] X. Liu, G. Zhao, Z. Chen, F. Panhwar, X. He, Dual suppression effect of magnetic induction heating and microencapsulation on ice crystallization enables low-cryoprotectant vitrification of stem cell-alginate hydrogel constructs, *ACS Appl. Mater. Interfaces* 10 (19) (2018) 16822–16835, doi:10.1021/acsm.8b04496.
- [130] F. Panhwar, Z. Chen, S.M.C. Hossain, M. Wang, Z. Haider, K. Memon, P. Chen, G. Zhao, Near-infrared laser mediated modulation of ice crystallization by two-dimensional nanosheets enables high-survival recovery of biological cells from cryogenic temperatures, *Nanoscale* 10 (25) (2018) 11760–11774, doi:10.1039/c8nr01349g.
- [131] L. Zhan, S.Z. Guo, J. Kangas, Q. Shao, M. Shiao, K. Khosla, W.C. Low, M.C. McAlpine, J. Bischof, Conduction cooling and plasmonic heating dramatically increase droplet vitrification volumes for cell cryopreservation, *Adv. Sci.* 8 (11) (2021) 2004605, doi:10.1002/advs.202004605.
- [132] C. Budke, C. Heggemann, M. Koch, N. Sewald, T. Koop, Ice recrystallization kinetics in the presence of synthetic antifreeze glycoprotein analogues using the framework of LSW theory, *J. Phys. Chem. B* 113 (9) (2009) 2865–2873, doi:10.1021/jp805726e.
- [133] I.K. Voets, From ice-binding proteins to bio-inspired antifreeze materials, *Soft Matter* 13 (28) (2017) 4808–4823, doi:10.1039/c6sm02867e.
- [134] C.A. Knight, D. Wen, R.A. Laursen, Nonequilibrium antifreeze peptides and the recrystallization of ice, *Cryobiology* 32 (1) (1995) 23–34, doi:10.1006/cryo.1995.1002.
- [135] P.W. Voorhees, The theory of ostwald ripening, *J. Stat. Phys.* 38 (1–2) (1985) 231–252, doi:10.1007/bf01017860.
- [136] A. Baldan, Progress in ostwald ripening theories and their applications to nickel-base superalloys, *J. Mater. Sci.* 37 (11) (2002) 2171–2202, doi:10.1023/a:1015388912729.
- [137] J. Chantelle, D. Malay, N. Robert, *Ice Recrystallization Inhibitors: From Biological Antifreezes to Small Molecules*, InTech New York, NY, 2013, pp. 177–224.
- [138] I.M. Lifshitz, V.V. Slyozov, The kinetics of precipitation from supersaturated solid solutions, *J. Phys. Chem. Solids* 19 (1–2) (1961) 35–50, doi:10.1016/0022-3697(61)90054-3.
- [139] C. Wagner, Theorie der alterung von niederschlägen durch umlösen (ostwald reifung), *Z. Phys. Chem.* 65 (78) (1961) 581–591, doi:10.1002/zppc.19610650704.
- [140] P.L. Davies, Ice-binding proteins: a remarkable diversity of structures for stopping and starting ice growth, *Trends Biochem. Sci.* 39 (11) (2014) 548–555, doi:10.1016/j.tibs.2014.09.005.
- [141] C.I. Biggs, T.L. Bailey, B. Graham, C. Stubbs, A. Fayter, M.I. Gibson, Polymer mimics of biomacromolecular antifreezes, *Nat. Commun.* 8 (2017) 1546, doi:10.1038/s41467-017-01421-7.
- [142] A. Ampaw, T.A. Charlton, J.G. Briard, R.N. Ben, Designing the next generation of cryoprotectants - from proteins to small molecules, *Pept. Sci.* 111 (1) (2019) e24086, doi:10.1002/pep2.24086.
- [143] L.L. Olijve, K. Meister, A.L. DeVries, J.G. Duman, S. Guo, H.J. Bakker, I.K. Voets, Blocking rapid ice crystal growth through nonbasal plane adsorption of antifreeze proteins, *Proc. Natl. Acad. Sci. U.S.A.* 113 (14) (2016) 3740–3745, doi:10.1073/pnas.1524109113.
- [144] R.Y. Tam, S.S. Ferreira, P. Czechura, J.L. Chaytor, R.N. Ben, Hydration index—a better parameter for explaining small molecule hydration in inhibition of ice recrystallization, *J. Am. Chem. Soc.* 130 (51) (2008) 17494–17501, doi:10.1021/ja806284x.
- [145] K. Röttger, A. Endriss, J. Ihringer, S. Doyle, W.F. Kuhs, Lattice constants and thermal expansion of H<sub>2</sub>O and D<sub>2</sub>O ice Ih between 10 and 265 K, *Acta Crystallogr. B. Struct. Sci. Cryst. Eng. Mater.* 50 (6) (1994) 644–648, doi:10.1107/s0108768194004933.

- [146] S.P. Graether, M.J. Kuiper, S.M. Gagne, V.K. Walker, Z. Jia, B.D. Sykes, P.L. Davies, Beta-helix structure and ice-binding properties of a hyperactive antifreeze protein from an insect, *Nature* 406 (6793) (2000) 325–328, doi:[10.1038/35018610](https://doi.org/10.1038/35018610).
- [147] Y.C. Liou, A. Tocilj, P.L. Davies, Z. Jia, Mimicry of ice structure by surface hydroxyls and water of a beta-helix antifreeze protein, *Nature* 406 (6793) (2000) 322–324, doi:[10.1038/35018604](https://doi.org/10.1038/35018604).
- [148] D.S. Yang, M. Sax, A. Chakrabarty, C.L. Hew, Crystal structure of an antifreeze polypeptide and its mechanistic implications, *Nature* 333 (6170) (1988) 232–237, doi:[10.1038/333232a0](https://doi.org/10.1038/333232a0).
- [149] C.A. Knight, C.C. Cheng, A.L. DeVries, Adsorption of alpha-helical antifreeze peptides on specific ice crystal surface planes, *Biophys. J.* 59 (2) (1991) 409–418, doi:[10.1016/s0006-3495\(91\)82234-2](https://doi.org/10.1016/s0006-3495(91)82234-2).
- [150] C.A. Knight, E. Driggers, A.L. DeVries, Adsorption to ice of fish antifreeze glycopeptides 7 and 8, *Biophys. J.* 64 (1) (1993) 252–259, doi:[10.1016/s0006-3495\(93\)81361-4](https://doi.org/10.1016/s0006-3495(93)81361-4).
- [151] Y. Yeh, R.E. Feeney, Antifreeze proteins: structures and mechanisms of function, *Chem. Rev.* 96 (2) (1996) 601–618, doi:[10.1021/cr950260c](https://doi.org/10.1021/cr950260c).
- [152] H. Geng, X. Liu, G. Shi, G. Bai, J. Ma, J. Chen, Z. Wu, Y. Song, H. Fang, J. Wang, Graphene oxide restricts growth and recrystallization of ice crystals, *Angew. Chem. Int. Ed. Engl.* 56 (4) (2017) 997–1001, doi:[10.1002/anie.201609230](https://doi.org/10.1002/anie.201609230).
- [153] G. Bai, Z. Song, H. Geng, D. Gao, K. Liu, S. Wu, W. Rao, L. Guo, J. Wang, Oxidized quasi-carbon nitride quantum dots inhibit ice growth, *Adv. Mater.* 29 (28) (2017) 1606843, doi:[10.1002/adma.201606843](https://doi.org/10.1002/adma.201606843).
- [154] G. Bai, D. Gao, J. Wang, Control of ice growth and recrystallization by sulphur-doped oxidized quasi-carbon nitride quantum dots, *Carbon* 124 (2017) 415–421, doi:[10.1016/j.carbon.2017.08.074](https://doi.org/10.1016/j.carbon.2017.08.074).
- [155] W. Zhu, J. Guo, J.O. Agola, J.G. Croissant, Z. Wang, J. Shang, E. Coker, B. Motewalli, A. Zimpel, S. Wuttke, C.J. Brinker, Metal-organic framework nanoparticle-assisted cryopreservation of red blood cells, *J. Am. Chem. Soc.* 141 (19) (2019) 7789–7796, doi:[10.1021/jacs.9b00992](https://doi.org/10.1021/jacs.9b00992).
- [156] P.L. Davies, J. Baardsnes, M.J. Kuiper, V.K. Walker, Structure and function of antifreeze proteins, *Philos. Trans. R. Soc. Lond., B, Biol. Sci.* 357 (1423) (2002) 927–935, doi:[10.1098/rstb.2002.1081](https://doi.org/10.1098/rstb.2002.1081).
- [157] Z. Jia, P.L. Davies, Antifreeze proteins: an unusual receptor ligand interaction, *Trends Biochem. Sci.* 27 (2) (2002) 101–106, doi:[10.1016/s0968-0004\(01\)02028-x](https://doi.org/10.1016/s0968-0004(01)02028-x).
- [158] M. Schauperl, M. Podewitz, T.S. Ortner, F. Waibl, A. Thoeny, T. Loerting, K.R. Liedl, Balance between hydration enthalpy and entropy is important for ice binding surfaces in antifreeze proteins, *Sci. Rep.* 7 (1) (2017) 11901, doi:[10.1038/s41598-017-11982-8](https://doi.org/10.1038/s41598-017-11982-8).
- [159] A.D.J. Haymet, L.G. Ward, M.M. Harding, Winter flounder “antifreeze” proteins: synthesis and ice growth inhibition of analogues that probe the relative importance of hydrophobic and hydrogen-bonding interactions, *J. Am. Chem. Soc.* 121 (5) (1999) 941–948, doi:[10.1021/ja9801341](https://doi.org/10.1021/ja9801341).
- [160] T. Congdon, R. Notman, M.I. Gibson, Antifreeze (glyco)protein mimetic behavior of poly(vinyl alcohol): detailed structure ice recrystallization inhibition activity study, *Biomacromolecules* 14 (5) (2013) 1578–1586, doi:[10.1021/bm400217j](https://doi.org/10.1021/bm400217j).
- [161] K. Mochizuki, V. Molinero, Antifreeze glycoproteins bind reversibly to ice via hydrophobic groups, *J. Am. Chem. Soc.* 140 (14) (2018) 4803–4811, doi:[10.1021/jacs.7b13630](https://doi.org/10.1021/jacs.7b13630).
- [162] A. Hudait, Y. Qiu, N. Odendahl, V. Molinero, Hydrogen-bonding and hydrophobic groups contribute equally to the binding of hyperactive antifreeze and ice-nucleating proteins to ice, *J. Am. Chem. Soc.* 141 (19) (2019) 7887–7898, doi:[10.1021/jacs.9b02248](https://doi.org/10.1021/jacs.9b02248).
- [163] R.C. Deller, M. Vatish, D.A. Mitchell, M.I. Gibson, Synthetic polymers enable non-vitreous cellular cryopreservation by reducing ice crystal growth during thawing, *Nat. Commun.* 5 (2014) 3244, doi:[10.1038/ncomms4244](https://doi.org/10.1038/ncomms4244).
- [164] P.M. Naullage, V. Molinero, Slow propagation of ice binding limits the ice-recrystallization inhibition efficiency of pva and other flexible polymers, *J. Am. Chem. Soc.* 142 (9) (2020) 4356–4366, doi:[10.1021/jacs.9b12943](https://doi.org/10.1021/jacs.9b12943).
- [165] F. Bachtiger, T.R. Congdon, C. Stubbs, M.I. Gibson, G.C. Sosso, The atomistic details of the ice recrystallisation inhibition activity of PVA, *Nat. Commun.* 12 (1) (2021) 1323, doi:[10.1038/s41467-021-21717-z](https://doi.org/10.1038/s41467-021-21717-z).
- [166] R.C. Deller, T. Congdon, M.A. Sahid, M. Morgan, M. Vatish, D.A. Mitchell, R. Notman, M.I. Gibson, Ice recrystallisation inhibition by polyols: comparison of molecular and macromolecular inhibitors and role of hydrophobic units, *Biomater. Sci.* 1 (5) (2013) 478–485, doi:[10.1039/c3bm00194f](https://doi.org/10.1039/c3bm00194f).
- [167] N. Smolin, V. Daggett, Formation of ice-like water structure on the surface of an antifreeze protein, *J. Phys. Chem. B* 112 (19) (2008) 6193–6202, doi:[10.1021/jp710546e](https://doi.org/10.1021/jp710546e).
- [168] C.P. Garnham, R.L. Campbell, P.L. Davies, Anchored clathrate waters bind antifreeze proteins to ice, *Proc. Natl. Acad. Sci. U.S.A.* 108 (18) (2011) 7363–7367, doi:[10.1073/pnas.1100429108](https://doi.org/10.1073/pnas.1100429108).
- [169] K. Meister, S. Strazdaitė, A.L. DeVries, S. Lotze, L.L. Olijve, I.K. Voets, H.J. Bakker, Observation of ice-like water layers at an aqueous protein surface, *Proc. Natl. Acad. Sci. U.S.A.* 111 (50) (2014) 17732–17736, doi:[10.1073/pnas.1414188111](https://doi.org/10.1073/pnas.1414188111).
- [170] S. Ebbinghaus, K. Meister, B. Born, A.L. DeVries, M. Gruebele, M. Havenith, Antifreeze glycoprotein activity correlates with long-range protein-water dynamics, *J. Am. Chem. Soc.* 132 (35) (2010) 12210–12211, doi:[10.1021/ja1051632](https://doi.org/10.1021/ja1051632).
- [171] K. Meister, S. Ebbinghaus, Y. Xu, J.G. Duman, A. DeVries, M. Gruebele, D.M. Leitner, M. Havenith, Long-range protein-water dynamics in hyperactive insect antifreeze proteins, *Proc. Natl. Acad. Sci. U.S.A.* 110 (5) (2013) 1617–1622, doi:[10.1073/pnas.1214911110](https://doi.org/10.1073/pnas.1214911110).
- [172] M. Heyden, E. Brundermann, U. Heugen, G. Niehues, D.M. Leitner, M. Havenith, Long-range influence of carbohydrates on the solvation dynamics of water—answers from terahertz absorption measurements and molecular modeling simulations, *J. Am. Chem. Soc.* 130 (17) (2008) 5773–5779, doi:[10.1021/ja0781083](https://doi.org/10.1021/ja0781083).
- [173] D.R. Nutt, J.C. Smith, Dual function of the hydration layer around an antifreeze protein revealed by atomistic molecular dynamics simulations, *J. Am. Chem. Soc.* 130 (39) (2008) 13066–13073, doi:[10.1021/ja8034027](https://doi.org/10.1021/ja8034027).
- [174] J.A. Raymond, A.L. DeVries, Adsorption inhibition as a mechanism of freezing resistance in polar fishes, *Proc. Natl. Acad. Sci. U.S.A.* 74 (6) (1977) 2589–2593, doi:[10.1073/pnas.74.6.2589](https://doi.org/10.1073/pnas.74.6.2589).
- [175] C.A. Knight, A.L. DeVries, Melting inhibition and superheating of ice by an antifreeze glycopeptide, *Science* 245 (4917) (1989) 505–507, doi:[10.1126/science.245.4917.505](https://doi.org/10.1126/science.245.4917.505).
- [176] Y. Celik, L.A. Graham, Y.F. Mok, M. Bar, P.L. Davies, I. Braslavsky, Superheating of ice crystals in antifreeze protein solutions, *Proc. Natl. Acad. Sci. U.S.A.* 107 (12) (2010) 5423–5428, doi:[10.1073/pnas.0909456107](https://doi.org/10.1073/pnas.0909456107).
- [177] N.H. Fletcher, *The Chemical Physics of Ice*, Cambridge University Press, Cambridge, 2010.
- [178] P. Wilson, Explaining thermal hysteresis by the kelvin effect, *CryoLetters* 14 (1993) 31–36.
- [179] M. Bar-Dolev, Y. Celik, J.S. Wettnaufer, P.L. Davies, I. Braslavsky, New insights into ice growth and melting modifications by antifreeze proteins, *J. R. Soc. Interface* 9 (77) (2012) 3249–3259, doi:[10.1098/rsif.2012.0388](https://doi.org/10.1098/rsif.2012.0388).
- [180] P. Czechura, R.Y. Tam, E. Dimitrijevic, A.V. Murphy, R.N. Ben, The importance of hydration for inhibiting ice recrystallization with c-linked antifreeze glycoproteins, *J. Am. Chem. Soc.* 130 (10) (2008) 2928–2929, doi:[10.1021/ja7103262](https://doi.org/10.1021/ja7103262).
- [181] M.J. Macielag, Chemical properties of antimicrobials and their uniqueness (2012) 793–820. 10.1007/978-1-4614-1400-1\_24
- [182] A. Eniade, M. Purushotham, R.N. Ben, J.B. Wang, K. Horwath, A serendipitous discovery of antifreeze protein-specific activity in C-linked antifreeze glycoprotein analogs, *Cell Biochem. Biophys.* 38 (2) (2003) 115–124, doi:[10.1385/cbb:38:2:115](https://doi.org/10.1385/cbb:38:2:115).
- [183] C.J. Capicciotti, M. Leclère, F.A. Perras, D.L. Bryce, H. Paulin, J. Harden, Y. Liu, R.N. Ben, Potent inhibition of ice recrystallization by low molecular weight carbohydrate-based surfactants and hydrogelators, *Chem. Sci.* 3 (5) (2012) 1408–1416, doi:[10.1039/c2sc00885h](https://doi.org/10.1039/c2sc00885h).
- [184] B. Graham, A.E.R. Fayter, J.E. Houston, R.C. Evans, M.I. Gibson, Facially amphiphatic glycopolymers inhibit ice recrystallization, *J. Am. Chem. Soc.* 140 (17) (2018) 5682–5685, doi:[10.1021/jacs.8b02066](https://doi.org/10.1021/jacs.8b02066).
- [185] D.E. Mitchell, G. Clarkson, D.J. Fox, R.A. Vipond, P. Scott, M.I. Gibson, Antifreeze protein mimetic metallohelices with potent ice recrystallization inhibition activity, *J. Am. Chem. Soc.* 139 (29) (2017) 9835–9838, doi:[10.1021/jacs.7b05822](https://doi.org/10.1021/jacs.7b05822).
- [186] C. Stubbs, T.L. Bailey, K. Murray, M.I. Gibson, Polyampholytes as emerging macromolecular cryoprotectants, *Biomacromolecules* 21 (1) (2020) 7–17, doi:[10.1021/acs.biomac.9b01053](https://doi.org/10.1021/acs.biomac.9b01053).
- [187] D.E. Mitchell, M. Lilliman, S.G. Spain, M.I. Gibson, Quantitative study on the antifreeze protein mimetic ice growth inhibition properties of poly(ampholytes) derived from vinyl-based polymers, *Biomater. Sci.* 2 (12) (2014) 1787–1795, doi:[10.1039/c4bm00153b](https://doi.org/10.1039/c4bm00153b).
- [188] K. Matsumura, F. Hayashi, T. Nagashima, R. Rajan, S.-H. Hyon, Molecular mechanisms of cell cryopreservation with polyampholytes studied by solid-state NMR, *Commun. Mater.* 2 (1) (2021) 15, doi:[10.1038/s43246-021-00118-1](https://doi.org/10.1038/s43246-021-00118-1).
- [189] W.F. Wolkers, H. Oldenhof, *Cryopreservation and Freeze-drying Protocols, Methods in Molecular Biology*, Springer, 2021.
- [190] C.A. Knight, J. Hallett, A.L. DeVries, Solute effects on ice recrystallization: an assessment technique, *Cryobiology* 25 (1) (1988) 55–60, doi:[10.1016/0011-2240\(88\)90020-x](https://doi.org/10.1016/0011-2240(88)90020-x).
- [191] C.I. Biggs, C. Stubbs, B. Graham, A.E.R. Fayter, M. Hasan, M.I. Gibson, Mimicking the ice recrystallization activity of biological antifreezes. when is a new polymer “active”? *Macromol. Biosci.* 19 (7) (2019) 1900082, doi:[10.1002/mabi.201900082](https://doi.org/10.1002/mabi.201900082).
- [192] M. Smallwood, D. Worrall, L. Byass, L. Elias, D. Ashford, C.J. Doucet, C. Holt, J. Telford, P. Lillford, D.J. Bowlers, Isolation and characterization of a novel antifreeze protein from carrot (*daucus carota*), *Biochem. J.* 340 (2) (1999) 385–391.
- [193] L.L.C. Olijve, A.S. Oude Vrielink, I.K. Voets, A simple and quantitative method to evaluate ice recrystallization kinetics using the circle hough transform algorithm, *Cryst. Growth Des.* 16 (8) (2016) 4190–4195, doi:[10.1021/acs.cgd.5b01637](https://doi.org/10.1021/acs.cgd.5b01637).
- [194] C. Budke, A. Dreyer, J. Jaeger, K. Gimpel, T. Berkemeier, A.S. Bonin, L. Nagel, C. Plattner, A.L. DeVries, N. Sewald, T. Koop, Quantitative efficacy classification of ice recrystallization inhibition agents, *Cryst. Growth Des.* 14 (9) (2014) 4285–4294, doi:[10.1021/cg5003308](https://doi.org/10.1021/cg5003308).
- [195] R.M.F. Tomas, T.L. Bailey, M. Hasan, M.I. Gibson, Extracellular antifreeze protein significantly enhances the cryopreservation of cell monolayers, *Biomacromolecules* 20 (10) (2019) 3864–3872, doi:[10.1021/acs.biomac.9b00951](https://doi.org/10.1021/acs.biomac.9b00951).
- [196] Y. Sun, D. Maltseva, J. Liu, n. Hooker T., V. Mailander, H. Ramlov, A.L. DeVries, M. Bonn, K. Meister, Ice recrystallization inhibition is insufficient to ex-

- plain cryopreservation abilities of antifreeze proteins, *Biomacromolecules* 23 (3) (2022) 1214–1220, doi:[10.1021/acs.biomac.1c01477](https://doi.org/10.1021/acs.biomac.1c01477).
- [197] H. Kawahara, S. Higa, H. Tatsukawa, H. Obata, Cryoprotection and cryosterilization effects of type I antifreeze protein on *e. coli* cells, *Biocontrol Sci.* 14 (2) (2009) 49–54, doi:[10.4265/bio.14.49](https://doi.org/10.4265/bio.14.49).
- [198] Y. Cao, M. Hassan, Y. Cheng, Z. Chen, M. Wang, X. Zhang, Z. Haider, G. Zhao, Multifunctional photo- and magnetoresponsive graphene oxide-fe3o4 nanocomposite-alginate hydrogel platform for ice recrystallization inhibition, *ACS Appl. Mater. Interfaces* 11 (13) (2019) 12379–12388, doi:[10.1021/acsmi.9b02887](https://doi.org/10.1021/acsmi.9b02887).
- [199] Z. Wang, B. Yang, Z. Chen, D. Liu, L. Jing, C. Gao, J. Li, Z. He, J. Wang, Bioinspired cryoprotectants of glucose-based carbon dots, *ACS Appl. Bio. Mater.* 3 (6) (2020) 3785–3791, doi:[10.1021/acsbm.0c00376](https://doi.org/10.1021/acsbm.0c00376).
- [200] T. Chang, O.A. Moses, C. Tian, H. Wang, L. Song, G. Zhao, Synergistic ice inhibition effect enhances rapid freezing cryopreservation with low concentration of cryoprotectants, *Adv. Sci.* 8 (6) (2021) 2003387, doi:[10.1002/advs.202003387](https://doi.org/10.1002/advs.202003387).
- [201] R.C. Deller, M. Vatish, D.A. Mitchell, M.I. Gibson, Glycerol-free cryopreservation of red blood cells enabled by ice-recrystallization-inhibiting polymers, *ACS Biomater. Sci. Eng.* 1 (9) (2015) 789–794, doi:[10.1021/acsbiomaterials.5b00162](https://doi.org/10.1021/acsbiomaterials.5b00162).
- [202] B. Graham, T.L. Bailey, J.R.J. Healey, M. Marcellini, S. Deville, M.I. Gibson, Polyproline as a minimal antifreeze protein mimic that enhances the cryopreservation of cell monolayers, *Angew. Chem. Int. Ed. Engl.* 56 (50) (2017) 15941–15944, doi:[10.1002/anie.201706703](https://doi.org/10.1002/anie.201706703).
- [203] Q. Qin, L. Zhao, Z. Liu, T. Liu, J. Qu, X. Zhang, R. Li, L. Yan, J. Yan, S. Jin, J. Wang, J. Qiao, Bioinspired l-proline oligomers for the cryopreservation of oocytes via controlling ice growth, *ACS Appl. Mater. Interfaces* 12 (16) (2020) 18352–18362, doi:[10.1021/acsmi.0c02719](https://doi.org/10.1021/acsmi.0c02719).
- [204] M. Leclerc, B.K. Kwok, L.K. Wu, D.S. Allan, R.N. Ben, C-linked antifreeze glycoprotein (C-AFGP) analogues as novel cryoprotectants, *Bioconjug. Chem.* 22 (9) (2011) 1804–1810, doi:[10.1021/bc2001837](https://doi.org/10.1021/bc2001837).
- [205] K. Matsumura, S.H. Hyon, Polyampholytes as low toxic efficient cryoprotective agents with antifreeze protein properties, *Biomaterials* 30 (27) (2009) 4842–4849, doi:[10.1016/j.biomaterials.2009.05.025](https://doi.org/10.1016/j.biomaterials.2009.05.025).
- [206] R. Rajan, M. Jain, K. Matsumura, Cryoprotective properties of completely synthetic polyampholytes via reversible addition-fragmentation chain transfer (raft) polymerization and the effects of hydrophobicity, *J. Biomater. Sci. Polym. Ed.* 24 (15) (2013) 1767–1780, doi:[10.1080/09205063.2013.801703](https://doi.org/10.1080/09205063.2013.801703).
- [207] J. Zhao, M.A. Johnson, R. Fisher, N.A.D. Burke, H.D.H. Stover, Synthetic polyampholytes as macromolecular cryoprotective agents, *Langmuir* 35 (5) (2019) 1807–1817, doi:[10.1021/acs.langmuir.8b01602](https://doi.org/10.1021/acs.langmuir.8b01602).
- [208] J.D. Huang, J.M. Guo, L. Zhou, G.S. Zheng, J.F. Cao, Z.Y. Li, Z. Zhou, L. Qi, C.J. Brinker, W. Zhu, Advanced nanomaterials-assisted cell cryopreservation: a mini review, *ACS Appl. Bio. Mater.* 4 (4) (2021) 2996–3014, doi:[10.1021/acsmi.1c00105](https://doi.org/10.1021/acsmi.1c00105).
- [209] C. Zhang, Y. Zhou, L. Zhang, L. Wu, Y. Chen, D. Xie, W. Chen, Hydrogel cryopreservation system: an effective method for cell storage, *Int. J. Mol. Sci.* 19 (11) (2018) 3330, doi:[10.3390/ijms19113330](https://doi.org/10.3390/ijms19113330).
- [210] Z. He, C. Wu, M. Hua, S. Wu, D. Wu, X. Zhu, J. Wang, X. He, Bioinspired multifunctional anti-icing hydrogel, *Matter* 2 (3) (2020) 723–734, doi:[10.1016/j.matt.2019.12.017](https://doi.org/10.1016/j.matt.2019.12.017).
- [211] Y.S. Song, D. Adler, F. Xu, E. Kayaalp, A. Nureddin, R.M. Anchan, R.L. Maas, U. Demirci, Vitrification and levitation of a liquid droplet on liquid nitrogen, *Proc. Natl. Acad. Sci. U.S.A.* 107 (10) (2010) 4596–4600, doi:[10.1073/pnas.0914059107](https://doi.org/10.1073/pnas.0914059107).
- [212] W. Rao, H. Huang, H. Wang, S. Zhao, J. Dumbleton, G. Zhao, X. He, Nanoparticle-mediated intracellular delivery enables cryopreservation of human adipose-derived stem cells using trehalose as the sole cryoprotector, *ACS Appl. Mater. Interfaces* 7 (8) (2015) 5017–5028, doi:[10.1021/acsmi.5b00655](https://doi.org/10.1021/acsmi.5b00655).
- [213] S. Stewart, X. He, Intracellular delivery of trehalose for cell banking, *Langmuir* 35 (23) (2019) 7414–7422, doi:[10.1021/acs.langmuir.8b02015](https://doi.org/10.1021/acs.langmuir.8b02015).
- [214] Y. Zhang, H. Wang, S. Stewart, B. Jiang, W. Ou, G. Zhao, X. He, Cold-responsive nanoparticle enables intracellular delivery and rapid release of trehalose for organic-solvent-free cryopreservation, *Nano Lett.* 19 (12) (2019) 9051–9061, doi:[10.1021/acsnanolett.9b04109](https://doi.org/10.1021/acsnanolett.9b04109).
- [215] G. Zhao, X. Liu, K. Zhu, X. He, Hydrogel encapsulation facilitates rapid-cooling cryopreservation of stem cell-laden core-shell microcapsules as cell-biomaterial constructs, *Adv Healthc Mater* 6 (23) (2017) 1700988, doi:[10.1002/adhm.201700988](https://doi.org/10.1002/adhm.201700988).
- [216] Y. Cheng, Y. Yu, Y. Zhang, G. Zhao, Y. Zhao, Cold-responsive nanocapsules enable the sole-cryoprotectant-trehalose cryopreservation of  $\beta$  cell-laden hydrogels for diabetes treatment, *Small* 15 (50) (2019) e1904290, doi:[10.1002/smll.201904290](https://doi.org/10.1002/smll.201904290).
- [217] W. Li, Z. Liu, C. Liu, Y. Guan, J. Ren, X. Qu, Manganese dioxide nanozymes as responsive cytoprotective shells for individual living cell encapsulation, *Angew. Chem. Int. Ed. Engl.* 56 (44) (2017) 13661–13665, doi:[10.1002/anie.201706910](https://doi.org/10.1002/anie.201706910).
- [218] G.M. Fahy, D.R. MacFarlane, C.A. Angell, H.T. Meryman, Vitrification as an approach to cryopreservation, *Cryobiology* 21 (4) (1984) 407–426, doi:[10.1016/0011-2240\(84\)90079-8](https://doi.org/10.1016/0011-2240(84)90079-8).
- [219] B.J. Murray, S.L. Broadley, T.W. Wilson, S.J. Bull, R.H. Wills, H.K. Christenson, E.J. Murray, Kinetics of the homogeneous freezing of water, *Phys. Chem. Chem. Phys.* 12 (35) (2010) 10380–10387, doi:[10.1039/c03297b](https://doi.org/10.1039/c03297b).
- [220] N.T. Thanh, N. Maclean, S. Mahiddine, Mechanisms of nucleation and growth of nanoparticles in solution, *Chem. Rev.* 114 (15) (2014) 7610–7630, doi:[10.1021/cr400544s](https://doi.org/10.1021/cr400544s).